Journal of Geophysical Research: Atmospheres

RESEARCH ARTICLE
10.1029/2017JD027652

Understanding the Dominant Sources and Tracks of Moisture for Summer Rainfall in the Southwest United States

Srijita Jana[1,2], Balaji Rajagopalan[1,2], Michael A. Alexander[3], and Andrea J. Ray[3]

[1]Department of Civil, Environmental and Architectural Engineering, University of Colorado Boulder, Boulder, CO, USA, [2]Cooperative Institute of Research in Environmental Sciences, University of Colorado Boulder, Boulder, CO, USA, [3]NOAA Earth System Research Laboratory, Boulder, CO, USA

Key Points:
- The leading source of moisture varies depending on the part of the region
- Land is an important source of moisture during the summer season
- Large-scale circulation features are consistent with major pathways of moisture

Supporting Information:
- Supporting Information S1
- Table S1
- Table S2

Correspondence to:
S. Jana and B. Rajagopalan,
srijita.jana@colorado.edu;
balajir@colorado.edu

Citation:
Jana, S., Rajagopalan, B., Alexander, M. A., & Ray, A. J. (2018). Understanding the dominant sources and tracks of moisture for summer rainfall in the southwest United States. *Journal of Geophysical Research: Atmospheres*, *123*, 4850–4870. https://doi.org/10.1029/2017JD027652

Received 13 SEP 2017
Accepted 15 APR 2018
Accepted article online 28 APR 2018
Published online 17 MAY 2018

Abstract We investigated the moisture sources and tracks that enable summer rainfall over the four-state southwestern U.S. region of Arizona, New Mexico, Colorado, and Utah by employing a high-resolution Lagrangian particle tracking model. Six locations were selected—Cedar City (Utah), Grand Junction (Colorado), Eastonville (Colorado), Laveen (Arizona), Redrock (New Mexico), and Melrose (New Mexico)—together, they represent six spatial regions of summer precipitation for the Southwest. Moisture tracks were generated for all the rainy days at these stations for the historical period 1979–2013. Tracks were generated for a 3-day period ending with the day of rainfall, which were then used to identify the source of moisture, pathway or trajectory, and the modulation along the track. The four major sources of moisture—Gulf of California, Gulf of Mexico (GoM), land, and the Pacific Ocean—were identified as responsible for summer rainfall over southwestern United States. The two dominant moisture sources at Laveen, Cedar City, Redrock, Grand Junction, and Eastonville were Gulf of California and land; at Melrose GoM and land were the dominant sources. The leading source of moisture at each location contributed to most of the extreme rainfall events. Tracks from GoM traveled the fastest and those from land sources were the slowest. Large-scale circulation features–pressure, convergence, and specific humidity–were consistent with the moisture tracks and were found to be strong throughout the 3-day period. This detailed and comprehensive generation of rainfall tracks offers unique insights into the moisture source and delivery for summer rainfall over southwestern United States.

1. Introduction

Summer (June–September) rainfall over the semiarid four-state southwest United States—Arizona, New Mexico, Utah, and Colorado—plays a significant role in the reliability of water resources. Annual precipitation in this region shows two maxima, one during the summer season and the other during the winter season. Winter precipitation in the Southwest provides close to 30% of the annual precipitation (Sheppard et al., 1999 and is mainly driven by midlatitude cyclonic systems. Summer precipitation, however, brings up to 50% of the annual rainfall in the southern parts of Arizona and New Mexico, which provides inflow to several rivers that are important for water supply, especially, the Colorado River, during the crucial dry season. Summer rainfall is highly variable and difficult to predict compared to its winter counterpart and is mostly produced by convective storms and tropical cyclones, influenced by the North American Monsoon (NAM) system (D. K. Adams & Comrie, 1997; Ropelewski et al., 2005).

Summer rainfall typically begins in June and lasts until mid-September in our study region (shown in Figure 1, described in section 2.1) that is bounded by the Gulf of California (GoC, hereafter) and the Pacific Ocean in the west, and the Gulf of Mexico (GoM, hereafter) in the east. The interior topography also plays a significant role in modulating the amount of rainfall by limiting the penetration of marine moisture. During this period, much of the lower elevation zones, especially the Sonoran Desert, receive up to 90% of possible summer insolation and surface temperatures typically exceed 40°C. These warm land surfaces in combination with atmospheric moisture supplied by nearby maritime sources are conducive to the formation of a monsoon-like system. Around the beginning of July, a ridge, called the monsoon anticyclone or the monsoon high, starts to develop at the jet stream level (Carleton et al., 1990; Erfani & Mitchell, 2014; Higgins et al., 1998, 1999; Okabe, 1995). The monsoon high is accompanied by a reversal of surface winds over northern GoC from northwesterly to southeasterly and an abrupt increase in moisture in the form of gulf surges (J. L. Adams & Stensrud, 2007; M. W. Douglas & Leal, 2003; Mejia et al., 2010; Stensrud et al., 1997) or noctural low-level jets (Anderson

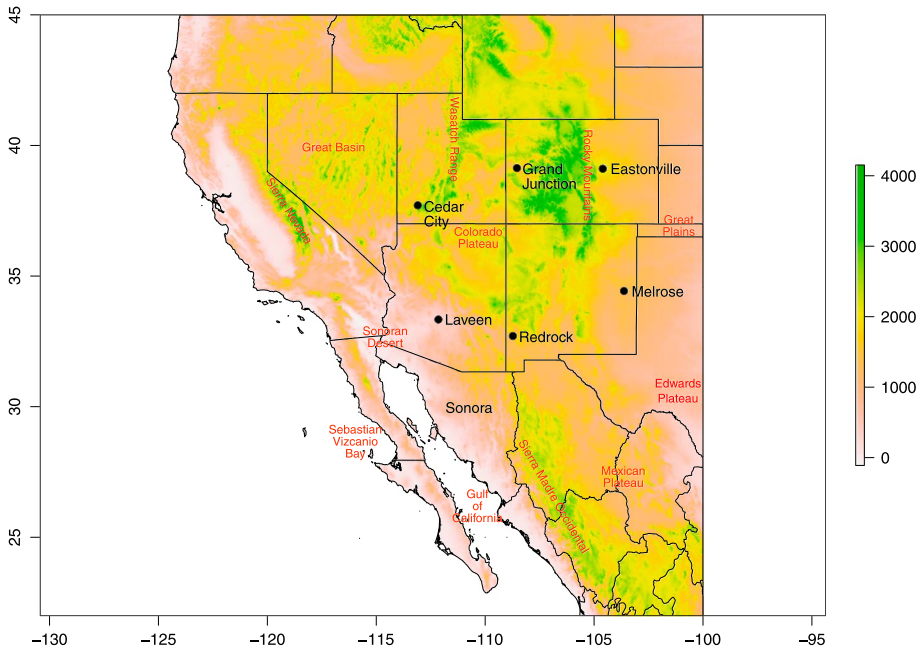

Figure 1. Topographic map (m, shading) of the western United States and Mexico. Representative stations selected for this study are shown as solid black circles and black text. Key topographical features referenced in this study are shown in red text.

et al., 2001; M. W. Douglas, 1995; M. W. Douglas et al., 1998). There is a concurrent increase in precipitation over the southwest United States, which coincides with the formation of the Arizona monsoon boundary (Adang & Gall, 1989). The onset of the monsoon in the southwest has been linked to an increase in rainfall along the East Coast of United States (Higgins et al., 1997) and a decrease in rainfall over the Great Plains (M. W. Douglas et al., 1993; Higgins et al., 1997; Mock, 1996). Between July and September, the NAM is fully developed and the northern edge extends into Arizona and New Mexico (M. W. Douglas et al., 1993). By late September, the ridge weakens over the Southwest and the monsoon high starts retreating southward (Vera et al., 2006).

One of the first field programs to study moisture in the monsoon region was the Southwest Area Monsoon Project. This program investigated the thunderstorm environments in central Arizona, monsoon structure and moisture fluxes, and convective systems in Mexico for the period of July–August 1990 (Meitin et al., 1991; Reyes et al., 1994). In the summer of 2004, the World Climate Research Programme/Climate Variability and Predictability/Variability of the American Monsoon Systems implemented a major field campaign called the NAM Experiment to determine the sources and limits of predictability of summer precipitation (Higgins et al., 2006). Following these field programs, two more recent programs—NAM Global Positioning System (GPS) Transect Experiment 2013 (Serra et al., 2016) and the NAM GPS Hydrometeorological Network 2017 (D. K. Adams et al., 2018)—have sought to quantify water vapor fluxes to improve the understanding of convection and hydrological cycle in the monsoon region. Although there have been several research efforts at understanding the moisture sources and pathways for summer rainfall in the core NAM region (approximately 24°–29°N, 109°–105°W), there has been a recent resurgence in interest in moisture sources, and moisture recycling in the extended monsoon region (D. K. Adams et al., 2018; Dominguez et al., 2016). Summer rainfall in the southwest United States is partly due to the weak northward extension of NAM, but it also exhibits independent variability due to several processes including mesoscale and synoptic disturbances and their interactions with topography. We refer our readers to D. K. Adams and Comrie (1997), Higgins et al. (1997), Barlow et al. (1998), and Vera et al. (2006) for a good overview of NAM and references within (Leung et al., 2003; Sheppard et al., 2002).

Of interest here are the moisture sources and pathways of summer rainfall in the southwestern United States. While the study region is primarily arid, these areas can receive significant summer precipitation that is

important for ecosystems, wildfire, and drought. The monsoon deep convection is also responsible for severe weather events in this region, such as strong winds, dust storms, lightning, hailstorms, and flooding. Although these events are highly localized, they can cause severe damage and losses (Maddox et al., 1995; Mazon et al., 2016). One such example is the multiday rainfall event over southeastern Arizona during 27–31 July 2006. During this event, upper-level steering winds swept multiple mesoscale convective systems over the same region over consecutive days, saturating the watersheds, which results in flooding (Griffiths et al., 2009).

Rainfall also affects the balance of summer supply and demand for many sectors ranging from wildlife to air quality management (Ray et al., 2007). In the past 60 years, there has been a long-term increase in atmospheric moisture and instability in the Southwest resulting in an increase in extreme monsoon precipitation (Luong et al., 2017), and thus, understanding the sources and delivery of moisture and moisture recycling is crucial. Additionally, the issue of moisture recycling is a large area of study and one that is critical for hydrometeorological studies. This research is motivated by these impacts of summer precipitation.

Based on the prevailing winds and geographic distribution of land-sea boundaries, early studies (Bryson, 1955; Jurwitz, 1953; Reitan, 1957) indicated GoM as the main source for moisture. Benton and Estoque (1954) analyzed water vapor transport over North America and found two well-defined moisture streams: southerly flow from the GoM and westerly flow from the Pacific Ocean. A similar analysis by Rasmusson (1966, 1967, 1968) concluded that water vapor west of the continental divide originates from the GoC. Hales (1972, 1974) proposed that surges of maritime tropical air travel into deserts of Arizona and California from the GoC. However, Brenner (1974) and Hales (1974) have expressed skepticism that moisture-laden flow from the GoM passing over the Sierra Madre Occidental (SMO) range (shown in Figure 1), which runs through northwestern and western Mexico, would still have a significant amount of moisture left when it arrived at Sonoran Desert. A recent study by Dominguez et al. (2016) using the Weather Research Forecasting model with water vapor diagnostics showed that low-level moisture in the Southwest comes from the GoC, which is the most important source whereas the upper-level moisture (above 800 hPa) comes from the GoM and SMO to the east. They also identified recycled moisture from within the monsoon region as the second most important source, contributing ~13% of the moisture to NAM precipitation.

Reyes and Cadet (1986, 1988) suggested that the intensification the South Pacific anticyclonic gyre and increase in southerly flux originating from the South Pacific Ocean is a major forcing mechanism for bringing low-level moisture along western Mexico. They also supported the findings of Rasmusson (1967), Hales (1972, 1974), Brenner (1974), and Tang and Reiter (1984) in calling the GoC a major moisture source for the southwest U.S. summer precipitation. Subsequently, several studies (Badan-Dangon et al., 1991; Bieda et al., 2009; Corbosiero et al., 2009; M. W. Douglas et al., 1993; M. W. Douglas, 1995) have used field data to provide further evidence for the transport from the GoC. These studies concluded that the transport from the GoC is more persistent because of the time-mean wind, and not short-lived surges as suggested by Hales (1972, 1974) and Brenner (1974). In another study, Carleton (1986) found that the rapid low-level surges from GoC in combination with the southeasterly moisture from GoM resulted in monsoon bursts in Arizona. For more detailed reviews of moisture sources for NAM precipitation, see M. W. Douglas et al. (1993, 1998), M. W. Douglas (1995), Stensrud et al. (1995, 1997), D. K. Adams and Comrie (1997), Hu and Dominguez (2015), and Dominguez et al. (2016).

GoC sea surface temperatures (SSTs) have also been found to play a crucial role in the development of the NAM system. Mitchell et al. (2002) found that the GoC SSTs along the mainland coast of Mexico should exceed 26°C for the northward advancement of precipitation. Warm SSTs off the west coast of Baja California have also been linked to wet monsoons in Arizona (Cavazos et al., 2002; Wright et al., 2001). Wright et al. (2001) found that higher SSTs cause increased vorticity, leading to increased transportation of moisture northward. Erfani and Mitchell (2014) have examined this mechanism using precipitation records, GoC SSTs, and high-resolution rawinsonde data. They found that before the onset of the monsoon the shallow boundary layer containing moist maritime air is trapped by drier, warmer air. But when the GoC temperatures rise above 29.5°C, the low-level inversion weakens and helps the moist air trapped in the boundary layer to mix with free tropospheric air. This results in a deep, moist layer that is then transported to the core NAM domain to form thunderstorms. It has also been observed in several

earlier studies (Mo & Juang, 2003; Stensrud et al., 1995) that models that underestimate GoC SSTs fail to reproduce realistic NAM simulations.

Terrestrial or continental sources have also been identified as an important moisture contributor. Isotopic methods or physical water vapor tracers have been used to distinguish between terrestrial and oceanic evaporative sources by several studies (Araguás-Araguás et al., 1998; Gimeno et al., 2012; Hu & Dominguez, 2015; Salati et al., 1979; Strong et al., 2007; Yamanaka et al., 2007). These studies, however, require intensive data on precipitation properties that are difficult to record or observe. Dirmeyer and Brubaker (1999) and Brubaker et al. (2001) developed a quasi-isentropic back trajectory scheme to estimate the evaporative source of observed precipitation in the Central United States. This scheme, however, fails to identify the rainfall causing air parcels in a vertical column.

Using water vapor tracer diagnostics in the NAM region, Bosilovich et al. (2003) observed that prior to monsoon onset, the Pacific Ocean and Mexican continental evaporation provided most of the moisture in the core monsoon region. After the onset, contribution of the Pacific reduces and local continental evaporation and the Atlantic Ocean become the dominant sources. During summers, high moisture recycling ratios in the range of 15–25% have been observed for the southwest United States, especially in eastern Colorado (Gimeno et al., 2012). Their hypothesis is that evapotranspiration provides moisture to the overlying atmosphere when large-scale advection decreases, such as the case in the northern regions of NAM. Moisture from the broader NAM region has also been linked to the adjacent plains via atmospheric hydrologic connectivity. During droughts, moisture advection from the Southwest can account for up to 15% of the summer rainfall in the adjacent Great Plains (Dominguez et al., 2009). On the contrary, Findell et al. (2011) observed land surface fluxes to have little control on local afternoon convection west of Mississippi. Recently, Bracken et al. (2015) also identified substantial moisture from land sources that produce precipitation extremes in several parts of the western United States in all seasons, in particular, the four-state Southwest region. Their study, however, did not separate the effect of evapotranspiration from the effect of large-scale moisture advected from the sea. The errors associated with humidity fields from reanalysis products and Lagrangian modeling are discussed in detail in sections 2.2 and 3, respectively.

Precipitation can also be modified by soil moisture variability and vegetation. Previous studies have shown that vegetation has a significant impact on monthly mean rainfall anomalies and even higher so on seasonal and longer time scales (Liu et al., 2006; Notaro et al., 2006). Alessandri and Navarra (2008) found that vegetation provides a delayed biophysical memory to large-scale atmospheric teleconnections such as El Niño–Southern Oscillation. Within the NAM region, Dominguez et al. (2008) found a positive feedback between precipitation and a subsequent increase in precipitation of recycled origin. They also found that evapotranspiration contributes significantly after the NAM onset and helps bring moisture to regions which would otherwise be dry. Precipitation during the monsoon onset leads to changes in vegetation that impact land surface states and fluxes (Méndez-Barroso & Vivoni, 2010). This positive vegetation-rainfall feedback is more important during periods of reduced large-scale moisture advection (Dominguez et al., 2008).

To resolve moisture sources and transport pathways, we use a Lagrangian model with high-resolution data that represents the complex topography for a relatively long period (1979–2013). These choices depart from previous studies; all of which were based on coarser models and limited time period. We analyze the moisture sources, transport pathways, steering characteristics, and their influence on precipitation amount and extremes, by developing moisture trajectories for all days with rainfall at several locations in the region. The terms "trajectories," "pathways," and "tracks" are used interchangeably in this paper. The paper is organized as follows: the data sets used in this study are first described in section 2, followed by the trajectory model used in identifying the sources and pathways in section 3. The results are then presented in section 4 followed by a summary and discussion in section 5.

2. Data

We used a combination of station rainfall data, large-scale atmospheric circulation fields, and backward trajectory models to identify moisture trajectories, their sources, and large-scale circulation features associated with summer rainfall events. The data sets used are described below, and the trajectory model is described in the following section.

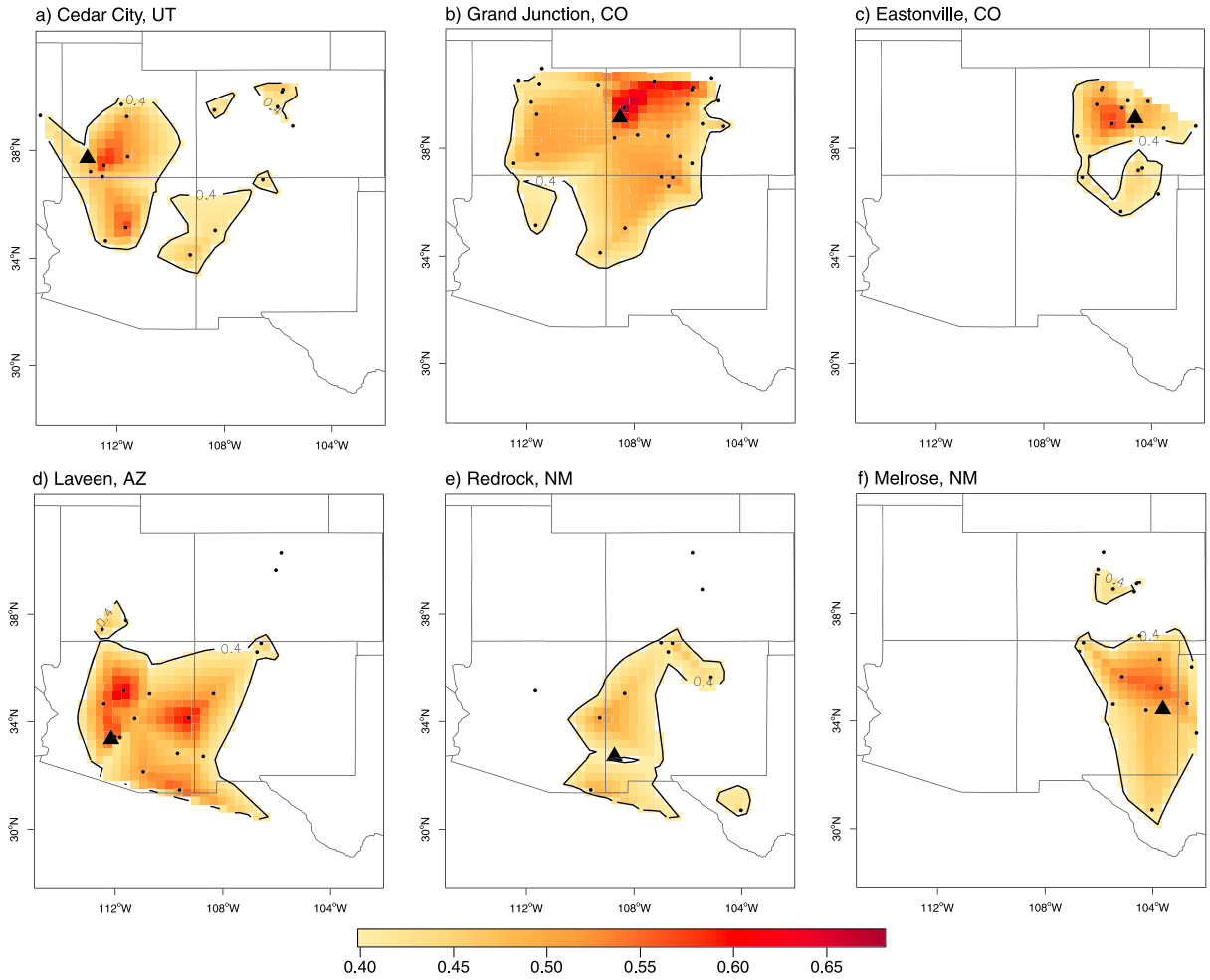

Figure 2. (a-f) JJAS conditional probability map of rainfall occurrence at a station given rainfall at a representative station. Black triangles indicate the location of the representative station, and black circles indicate the stations with a conditional probability greater than 0.4.

2.1. Station Precipitation Data

We obtained daily rainfall records at 73 stations covering the four-state southwest United States region of Utah, Colorado, Arizona, and New Mexico for the period 1979–2013 from the Global Daily Climatology Network data set (http://www.ncdc.noaa.gov/oa/climate/research/gdcn/gdcn.html) (Easterling, 2002). We used six stations (shown as black solid circles in Figure 1) to represent the five spatial regions delineated by Gutzler (2004) for early and late summer monsoon seasons: Cedar City (Utah) represents the intermountain region, Grand Junction (Colorado) represents the western slope of the Rocky Mountains, Laveen (Arizona) represents the arid parts of Arizona, Redrock (New Mexico) represents the core monsoon region, and Eastonville (Colorado) and Melrose (New Mexico) represent the plains. To demonstrate that these stations collectively capture the southwest United States, in Figure 2 we show the conditional probability of rainfall occurrence for the full season at other stations given the occurrence of rainfall at a representative station, regions with probability greater than 0.4 are shaded. The conditional probability maps for individual months are shown in Figures S2–S7 in the supporting information. The rainfall occurrence is defined as rainfall greater than 10 mm. Cedar City had 462 such rainfall events between 1979 and 2013; Eastonville had 793 and Melrose had 828 rainfall events. About 60% of rainfall events at these three stations occurred during the months of July and August. Laveen and Redrock had 253 and 815 rainfall events respectively with ~70% of these events occurred in the months of July and August. For the extreme events, we selected all rainfall events above the 85th percentile at each station. Cedar City had 69 extreme rainfall events during the period 1979–2013, Eastonville 129, Laveen 39, Redrock 118 and Melrose had 122 such events. The spatial extent of

correlated regions (i.e., the shaded regions) for all the five locations collectively captures the entire four-state southwestern United States, although there is some overlap between the regions that the stations represent.

2.2. North American Regional Reanalysis

Large-scale atmospheric fields that are necessary for computing trajectories were obtained from the National Centers for Environmental Prediction (NCEP) North American Regional Reanalysis (NARR) data set (Mesinger et al., 2006) for the period 1979–2013. NARR is a model product that assimilates several observational data sets to improve model performance, such as ground-based, dropsonde, rawinsonde, aircraft, satellite, and ship data. Disaggregated precipitation data for assimilation come from a 1° rain gauge analysis for Mexico and Canada, a 0.125° rain gauge analysis for continental United States, and the Climate Prediction Center (CPC) Merged Analysis of Precipitation for oceans south of 27.5°N and land areas south of Mexico. For areas north of 42.5°N, there is no assimilation due to lack of reliable CPC Merged Analysis of Precipitation data (Mesinger et al., 2006).

The model is run using the 2003 high-resolution version of the NCEP Eta Model (32 km per 45 layers) together with the associated Eta Data Assimilation System. The Eta model is coupled with the Noah land surface model (Ek et al., 2003) to produce simulations of land surface temperature, components of surface energy balance and surface water balance, and the evolution of soil temperature and soil moisture. The model drives latent heating profiles from precipitation analyses as forcings to produce NARR precipitation data (Lin et al., 1999). This assimilation, however, produces imbalances between the atmosphere and land surface models, which in turn affects the modeled soil moisture and evaporation (Dominguez & Kumar, 2008; Leeper et al., 2017). Precipitation from NARR has been compared to observed and gridded data sets in several studies. Becker et al. (2009) compared the NARR seasonal mean to gridded precipitation and found that the two data sets were in good agreement throughout the year but NARR was unable to capture convective storms during the summer. Bukovsky and Karoly (2007) studied the spatial distributions, diurnal cycle, and the annual cycle of precipitation for the whole United States and found the NARR data set to perform better than other reanalyses products. Leeper et al. (2017), however, found NARR modeled precipitation to be systematically lesser than the observed precipitation at U.S. Climate Reference Network stations. Despite these biases, NARR was able to capture the signal of the 2012 drought, including the timing, intensity, and spatial extent. NARR was also able to represent the winter moisture transport in the U.S. well but it failed to do so in summer. In summer, there is considerable difference between the global and regional reanalyses for summer flux convergence over Gulf Coast and the Great Plains (Nigam & Ruiz-Barradas, 2006).

A comparison of relative humidity fields from NARR with soundings from the Atmospheric Radiation Measurement Program by Kennedy et al. (2011) showed that the NARR relative humidity field is in good agreement with observations, with differences near the top of the troposphere during the summer. Radhakrishna et al. (2015) compared spatial maps of column-averaged mixing ratios (CAMRs) derived from integrated precipitable water from observations and NARR. They found NARR to have high correlation with the observations on monthly and annual scales. On annual scale, NARR was also able to resolve the high variability in moisture associated with NAM. But NARR does not correctly simulate diurnal cycle over the Rockies and western United States. During the daytime, CAMR values from reanalysis increased with time and then dropped at 0000 UTC. The increase in CAMR was due to either excessive surface evaporation or improper accounting for transport of moisture and for precipitation. For this study, meteorological fields such as geopotential heights, winds, temperature, and relative humidity on a 3-hourly, 32-km grid with 29 pressure levels were obtained from NARR. Also, the time-invariant land mask (land or water) from NARR was used in the identification of trajectory sources, described in section 3.

2.3. Climate Forecast System Reanalysis

Large-scale atmospheric fields for creating composite maps of 500-hPa geopotential height, 700-hPa specific humidity, integrated vapor transport (IVT), and convergence were obtained from the NCEP Climate Forecast System Reanalysis (CFSR) data set (Saha et al., 2010) for the period 1979–2010. We computed the IVT as the integral of winds and specific humidity from the surface to 300-hPa pressure level at 6-hourly intervals during summer (June–September).

The CFSR data set is available on a 6-hourly, 38-km (T382) grid and archived at 0.5° resolution at 64 pressure levels on a global scale, hence allowing us to extend the analysis beyond the NARR domain. This data set also includes atmospheric, oceanic, and land surface output products. Although the resolution of CFSR is relatively

fine compared to other reanalyses, it is still coarse to be able to represent the mountains in western U.S. well, and therefore, one should exercise caution when using the humidity field to model precipitation. A 32-year (1979–2010) monthly climatology was constructed for 500-hPa geopotential height, 700-hPa specific humidity, and total IVT, and the monthly anomalies were computed by subtracting the monthly climatology from the field.

3. Moisture Trajectories—HYSPLIT Model

There are three methods available for identifying sources and sinks of atmospheric moisture—analytical or box models, numerical water vapor tracers, and physical water vapor tracers or isotopes (Gimeno et al., 2012). Langrangian or trajectory-based models have been used in several studies to identify the geographical origin of moisture both globally (Dirmeyer & Brubaker, 2007; Stohl & James, 2005) and regionally (Nieto et al., 2006; Sodemann & Stohl, 2009). In this study, we used the Hybrid Single Particle Lagrangian Integrated Trajectory (HYSPLIT) model (Draxler et al., 2014; Draxler & Hess, 1997, 1998) developed by the National Oceanic and Atmospheric Administration Air Resources Laboratory to generate backward trajectories. HYSPLIT uses three-dimensional wind fields, pressure, temperature, and relative humidity from NARR, and it can be modified to provide additional output-like specific humidity, altitude (in meters above ground level, AGL), and pressure. The HYSPLIT model has been used widely to identify moisture sources of extreme precipitation over western United States (Bracken et al., 2015), to simulate intercontinental transport of pollution from North America (Stohl, 2003), in hurricane modeling (Stohl et al., 2008), and isotopic modeling of moisture at several locations including the southwest United States (Strong et al., 2007), and other regions around the world (Bottyán et al., 2014; Gustafsson et al., 2010; James et al., 2004).

The HYSPLIT model computes the advection of a particle or "puff" from the average of the three-dimensional velocity vectors for the initial position $P(t)$ and the first guess position $P'(t + \Delta t)$. The velocity vectors (V) are linearly interpolated in space and time. The first guess position is

$$P'(t + \Delta t) = P(t) + V(P, t)\Delta t,$$

and the final position is

$$P'(t + \Delta t) = P(t) + 0.5 * (V(P, t) + V(P', t + \Delta t))\Delta t.$$

This integration method was used for trajectory analysis notably by Petterssen (1940) and Draxler (1996) and is widely used.

Three-day backward trajectories were computed for every rainfall event (defined as days with rainfall greater than or equal to 10 mm) at each representative station. A 3-day period was chosen since most of the rainfall activity in summer is due to regional or local convective activity that develops over a relatively short period (Fuller & Stensrud, 2000). There is evidence of a dynamical transition in mid-August from smaller, subsynoptic scale to larger, synoptic scale moisture transport from previous studies (Kursinski et al., 2008). The trajectories were initiated from the station that recorded the rainfall event at four 6-hourly intervals on the day of the rainfall event. In the vertical level, trajectories were launched from 500 to 2,000 m (AGL) at 100-m increments. A total of 64 trajectories (16 height levels x 4 times per day) was initiated for each rainfall event. The trajectory position and specific humidity were computed backward in time at 1-hr intervals using the 3-hourly NARR wind, temperature, and humidity fields. During the 3-day period, a trajectory may undergo a series of evaporation and precipitation cycles before arriving at the target station. To select the trajectories that lost the highest amount of moisture closer to or at the target station, we removed the ones that dropped below the specific humidity level at hour 0 (time of the event) in the last 12 hr of their travel. Then, we selected the trajectory carrying the highest amount of moisture at hour 0. This was repeated for every rainfall event at a representative station. Previous studies such as Wernli and Davies (1997), Wernli (1997) have also used the decrease of specific humidity along a trajectory to estimate precipitation rates.

Using shorelines and the NARR land-sea mask, we defined three oceanic (GoC, GoM, and Pacific) and one terrestrial source (land) for moisture. Global coastlines were obtained from OpenStreetMap (OSM, http://openstreetmapdata.com/data/coastlines) developed under the OSMCoastline program. These regions are shown in supporting information Figure S1. The origin of a trajectory is defined as its location 72 hr prior to an event. If a trajectory originated from or had the highest specific humidity over an oceanic source, it was categorized

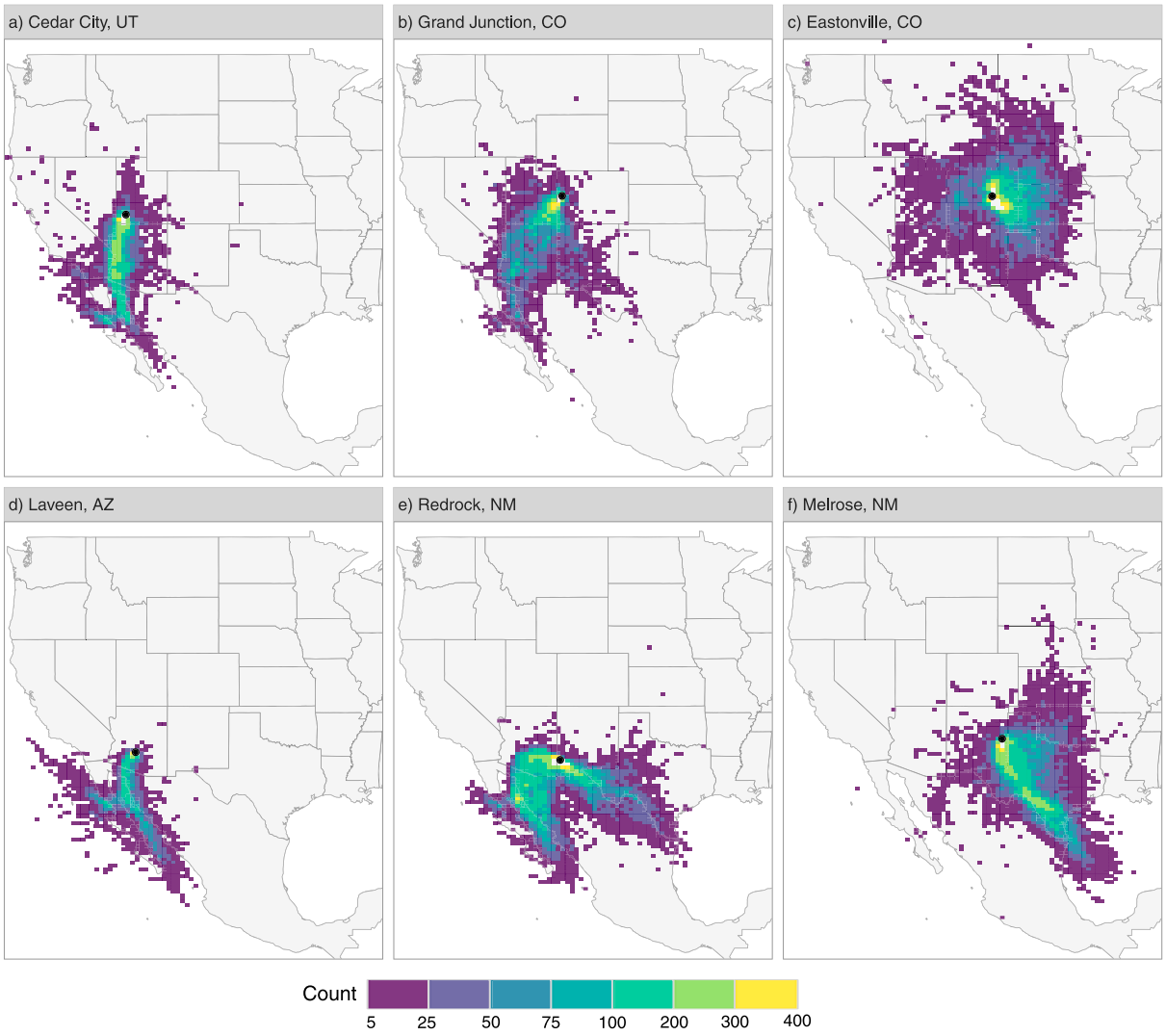

Figure 3. (a-f) Moisture trajectory counts for each station binned on the North American Regional Reanalysis native grid. Black solid circles indicate the location of the representative stations.

as coming from that oceanic source, else, it was a land trajectory. In this study, we do not distinguish between land trajectories resulting from soil moisture and those from evapotranspiration.

Although Lagrangian models like HYSPLIT allow for a quantitative interpretation of moisture origin and provide high spatial resolution moisture source diagnostics with realistic tracks of air parcels, they have several limitations of their own. In these models, evaporation rates are based on calculations rather than observations and separating evaporation from precipitation is not an easy task in some models (Stohl & James, 2004). They can, however, be improved by incorporating information on moist processes and convective mass flux along the parcel paths (Dirmeyer & Brubaker, 1999), but this is beyond the scope of our study. Another caveat of Lagrangian models is the usage of a time derivative of humidity along a particle trajectory. If the data contain random unrealistic fluctuations of humidity they would cancel out for longer time averages (Stohl & James, 2005). But on shorter time scales, these fluctuations can affect the trajectory path significantly. This makes relative humidity the most uncertain variable in our analysis. Thus, our results are sensitive to NARR errors and error propagation in the computation of trajectories, and there is a need to exercise caution when using NARR to simulate precipitation amounts.

For this study, we chose the NARR data set for four reasons. First, it has the highest resolution of all reanalyses available for running the HYSPLIT model. Second, since it assimilates precipitation and does

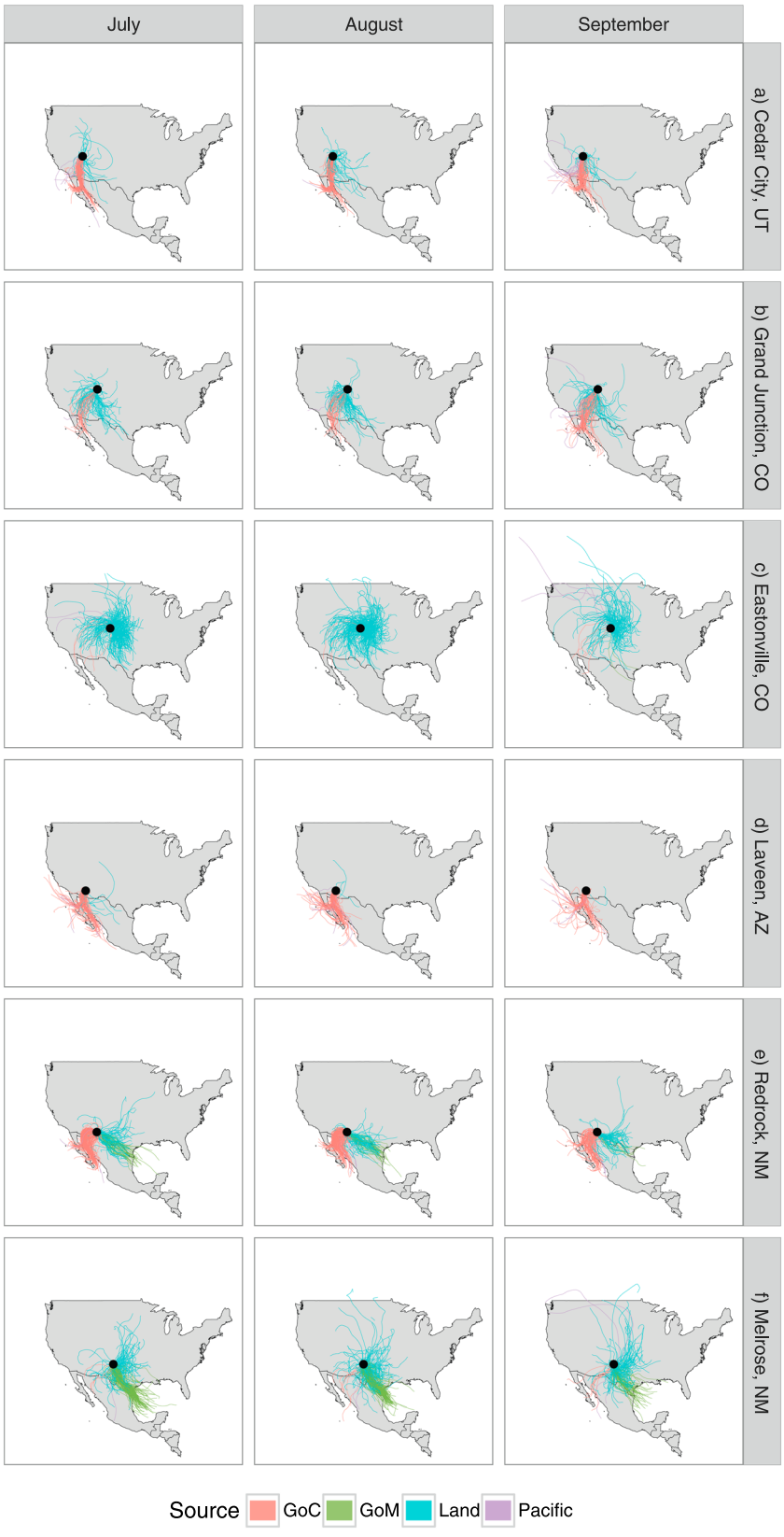

Figure 4. (a-f) Horizontal rain trajectories by month and station. Colors indicate the source of each trajectory. Black circles indicate the location of the representative stations.

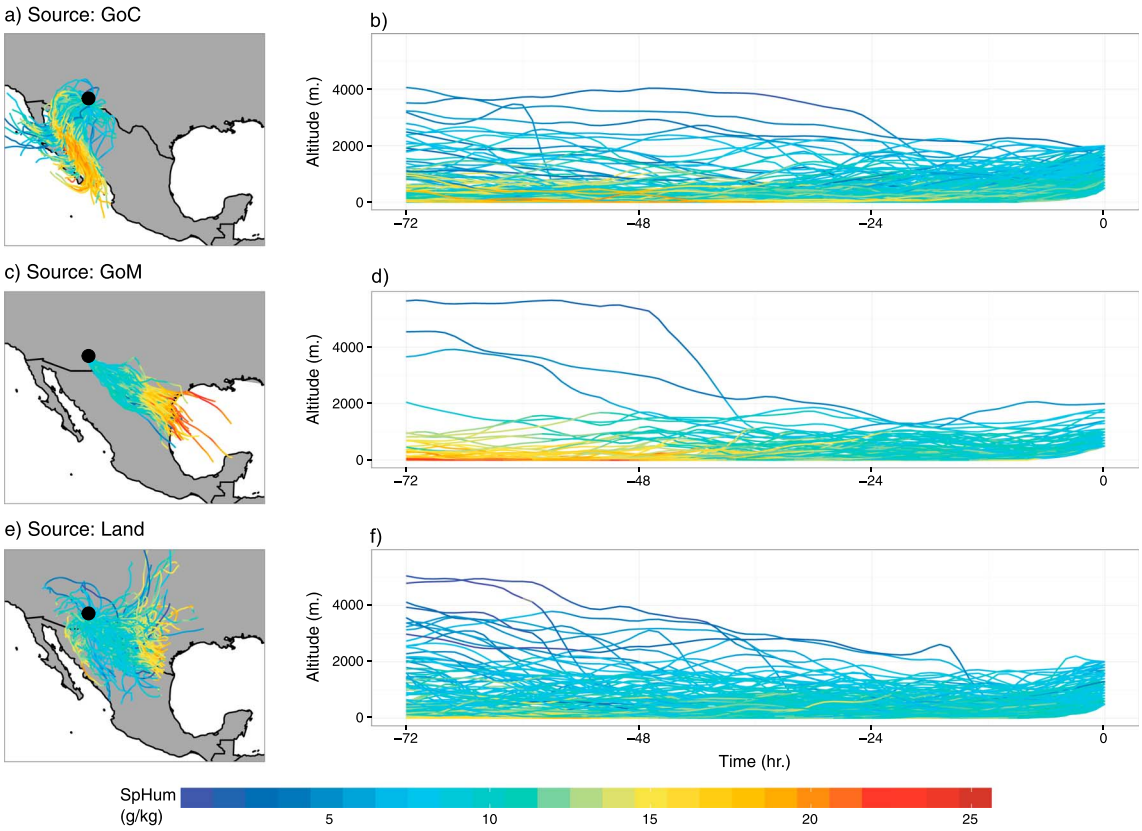

Figure 5. (a-f) Rain trajectories (for Redrock, NM) with the highest specific humidity (SpHum) at the time of the rainfall event. Color indicates the specific humidity in grams per kilograms. The left panel shows the horizontal location of the trajectories, and the right panel shows the altitude (height above ground level) of the trajectories as a function of time. Black circle indicates the location of Redrock, NM.

not use a parameterization scheme, the moisture representation is better than some other reanalyses (Ruiz-Barradas & Nigam, 2006, 2013). Third, for generating trajectories, we need a 3-D gridded wind product, which is not possible with in situ data or satellite products. And lastly, reanalyses products are known to be dynamically constrained.

4. Results

The horizontal trajectories for the representative stations along with their sources, frequencies, and speeds are presented followed by a description of the large-scale circulation fields associated with moisture delivery to the different areas in the southwest United States. Based on these results, we put forward a hypothesis for the moisture delivery into southwest United States.

4.1. Pathways and Sources

Trajectory counts for each station on the NARR native grid provide insights into the pathways and are presented in Figure 3. The count map for Cedar City (Figure 3a) shows that the greatest number of trajectories arrive from the south through the GoC, with some originating in the Gulf and others moving over Sebastian Vizcaino Bay, located at ~28°N on the west side of Baja California, to the GoC. The second highest set of trajectories is from the Pacific, arriving at the station via south of Sierra Nevada mountain range and through the Mojave Desert.

For Grand Junction (Figure 3b), the highest number of trajectories originated from the GoC and some from the northern part of the core NAM domain. For Eastonville (Figure 3c) in eastern Colorado, almost all of the trajectories originated over land, and a modest number of them originated from the south, extending to the GoM in the south. At Laveen (Figure 3d), majority of the trajectories traveled from the GoC and, similar to Cedar City (Figure 3a), some originated over the GoC while others originated over the Pacific and traversed

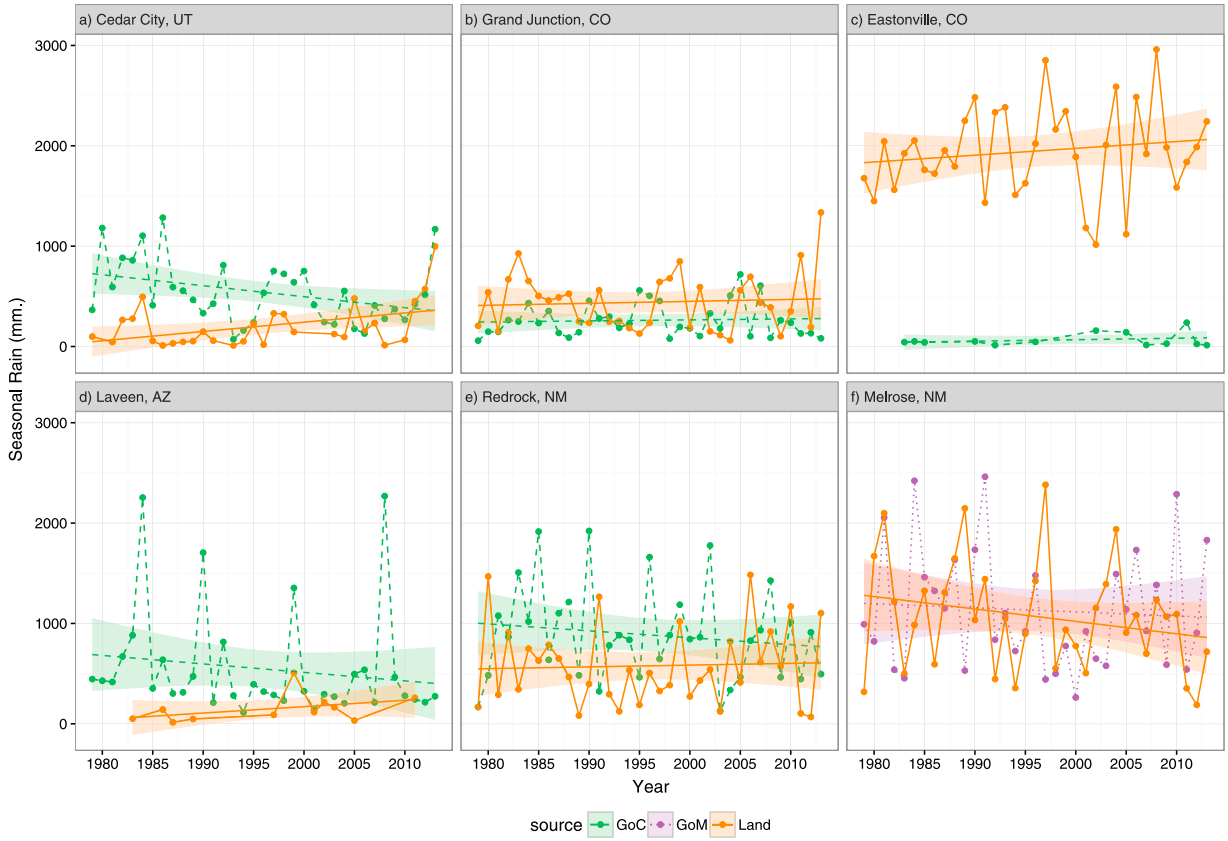

Figure 6. (a-f) Amount of JJAS rainfall (mm) associated with rain trajectories coming from a single source, as a function of time. Line color and line type indicate the source of the rain trajectory; the shaded region indicates the outer bounds for 0.95 level of confidence interval.

the Sebastian Vizcaino Bay. The count map for Redrock (Figure 3e) shows two prominent pathways of moisture: one is through the Mexican state of Sonora after traveling over the GoC, and the second pathway is upstream along the Rio Grande River originating from the GoM. The count map for Melrose (Figure 3f) shows that the highest number of trajectories moved inland from the GoM through the Edwards Plateau in west central Texas. The counts for pathways producing extreme rainfall events (defined as days with rainfall above the 85th percentile) were similar to those seen in Figure 3 and are shown in the supporting information (Figure S8).

The trajectories at the six representative stations during the individual months (July, August, and September) are shown in Figure 4. The sources of these trajectories are the same during all the months, except that the frequency is higher during the peak monsoon season (July–August). The frequency of trajectories for all the precipitation events and extreme events are listed in Table S1. This table helps identify the first and second dominant source of moisture for each station.

4.2. Altitude Profiles

Moisture trajectories for all rainfall events at Redrock are shown in Figure 5 along with their altitude profiles, to understand the height above the local topography at which moisture is picked up and transported. The trajectories categorized as GoC that help bring rainfall to Redrock are shown in Figure 5a. The general trend of these trajectories is to travel eastward from the Pacific Ocean into the GoC and then move northward into Sonora. These trajectories originating from the Pacific have the highest specific humidity in the GoC region, as shown by the orange lines with increasing humidity closer to the event (time = 0) in the right-hand side panel. The trajectories with high levels of specific humidity traveled closer to the ground (within 500–1,000 m).

The trajectories originating in the GoM arriving at Redrock are shown in Figure 5b. These trajectories have the highest specific humidity over the GoM at the origin, and they start to lose moisture as they travel over land—

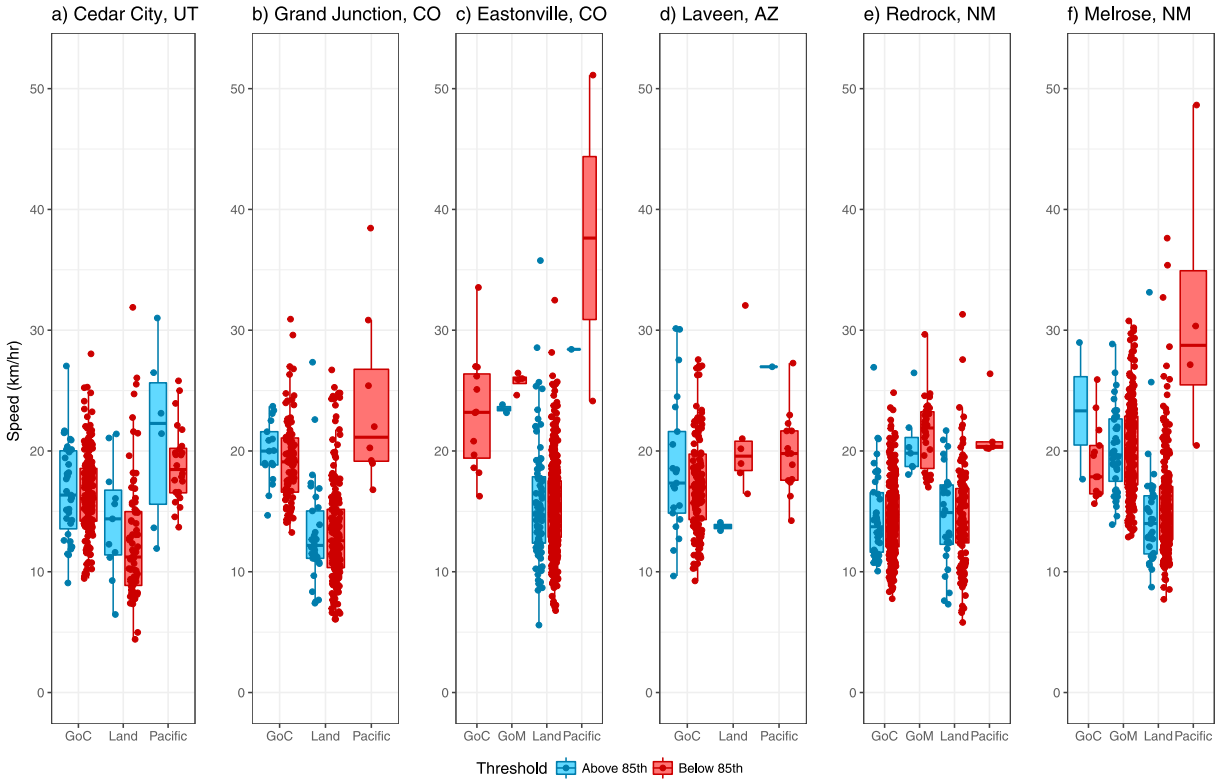

Figure 7. (a-f) Overall speed of rain trajectories by station. Color of the boxplot indicates the category of the rainfall event: Below 85th percentile (red) and above 85th percentile (blue). The width of the boxes is not indicative of any modeling variable.

as seen in the right-hand panel, high specific humidity at time = −72 hr and reducing closer to the location. The trajectories carrying the most moisture, or those with highest specific humidity, traveled close to the ground, similar to what we observed in Figure 5a. The trajectories originating from land are shown in Figure 5c. Land trajectories were seen to have higher levels of humidity when traveling from the east.

The general trend observed in the vertical profiles of trajectories from all sources is that they tend to ascend as they approach Redrock. This typically happens in the last 6 hr of trajectory travel, suggesting that the trajectories might be forced up to go over the topography and the additional heating provided by latent heat release would force the air parcel to rise. Similar behavior was observed by Gustafsson et al. (2010) for trajectories in Southern Sweden.

The trajectories and their altitude profiles for other stations are shown in Figures S9–S13. The middle-latitude and high-latitude Pacific trajectories in these figures show a common trend; they tend to have much lower levels of moisture compared to the GoC and GoM trajectories. The waters off the coast of California are very cold (20–21°C) and further south of California and west of Baja; the waters can be 5–10° colder than the water in GoC. But the Pacific can still be a contributor of moisture if the air parcel originates further south and west where the ocean is warmer. This is consistent with the findings of Hu and Dominguez (2015) in that the moisture contribution from the middle and high Pacific are smaller in comparison to eastern tropical Pacific, GoC, Atlantic, and the terrestrial sources.

Trajectories from all the stations show similar behavior in the last 6 hr of travel, in that they tend to ascend. The land as a source for precipitation extremes in the western United States has been recently reported (Bracken et al., 2015), which is consistent with our finding that terrestrial and atmospheric moisture recycling can contribute significantly to summer rainfall. However, it should be noted that prior to July, the vegetation and soils in Sonora, Chihuahua, and Northern Baja California are very dry and not conducive of any effective large-scale land surface water vapor fluxes. Once the monsoon sets in, in the first week of July, the evapotranspiration due to greening of vegetation increases (Vivoni et al., 2008) and so does the moisture transport northward.

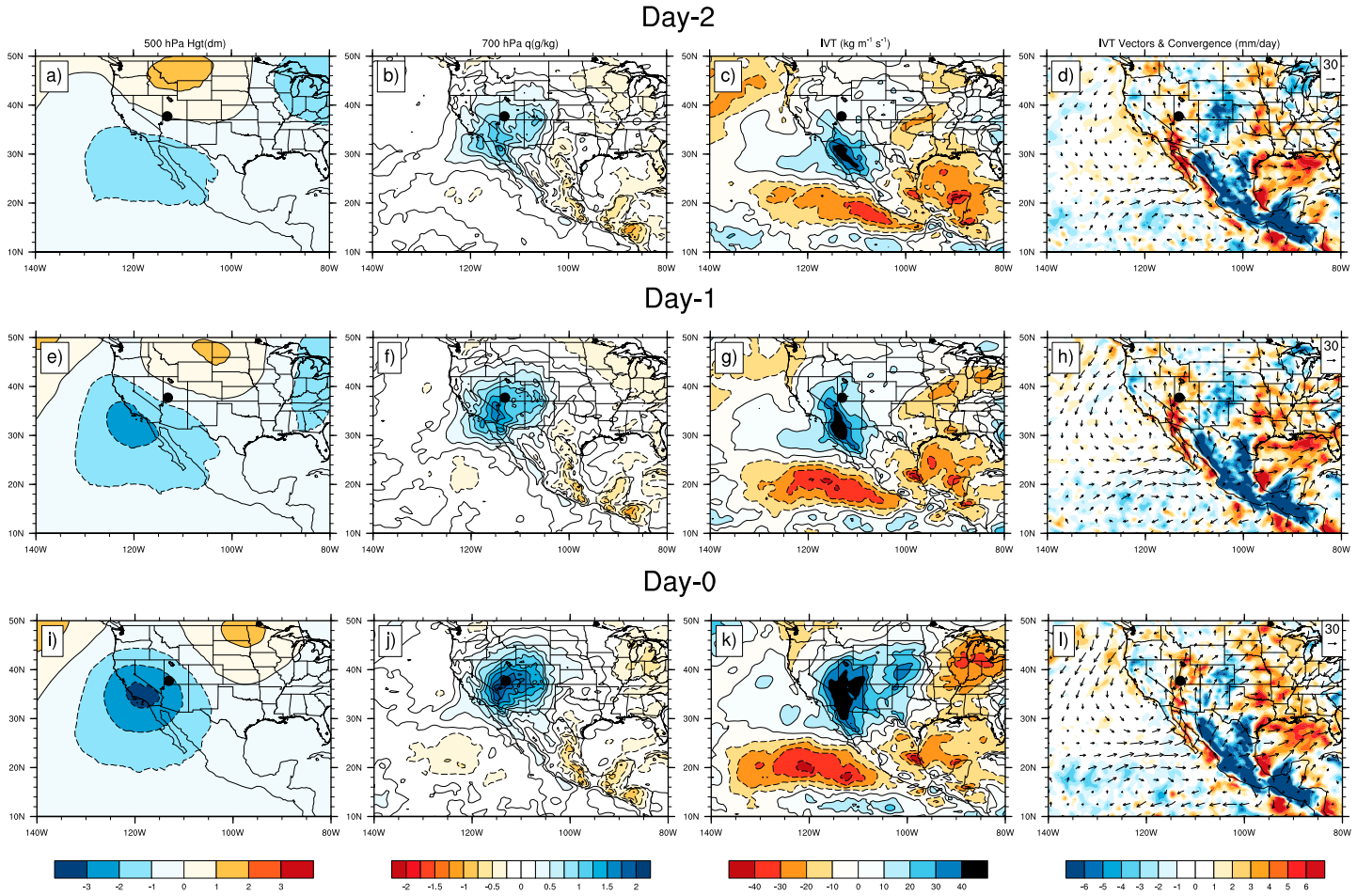

Figure 8. Composite maps of rainfall events for Cedar City, UT originating from GoC of anomalous (a) 500-hPa geopotential height (contour, 1 dm), (b) 700-hPa specific humidity (contour, 0.25 g/kg), (c) total IVT (contour, 10 kg · m^{-1} · s^{-1}), and (d) integrated vapor transport vectors and moisture convergence (color, mm/day) from Climate Forecast System Reanalysis on Day-2 (2 days prior to rainfall events). (e)–h) same as (a)–(d) but for Day-1 (1 day prior to rainfall events). (i)–(l) same as (a)–(d) but for day 0 (the day of the rainfall events). Solid black circle shows the location of the station.

4.3. Moisture Source and Rainfall Trends

We computed the total seasonal rainfall associated with the two dominant moisture sources—delivered at each of the representative stations—and show their temporal trends in Figure 6. The two dominant sources for rainfall trajectories at both Cedar City and Laveen are GoC and land (shown in Figures 6a and 6d). Annual rainfall totals from GoC followed a decreasing trend, while the totals from land showed an increase. The slopes and *p* values of linear-fitted models for the annual frequencies are presented in Table S2. Out of the six stations, the trends for only Cedar City were found to be statistically significant at the 95% confidence level. There is no trend in the rainfall from GoC and land sources that provide rainfall to Grand Junction (Figure 6b). For Eastonville (shown in Figure 6c), the two dominant sources are land and GoC. Land trajectories show an increase in the amount of rainfall delivered over time but the rainfall from GoC trajectories contribute minimal amounts and show no trend. Figure 6e shows the rainfall totals from the two dominant sources, GoC, and land, for Redrock in New Mexico. While the totals from GoC followed a downward trend, those from the land showed a steady increase. Figure 6f shows the rainfall totals from GoM and land for rain trajectories in Melrose. Melrose is the only station with decreasing rainfall from land trajectories. The increase in rainfall from land trajectories across almost the entire region could be due to several reasons—(i) increased moisture recycling due to increasing temperatures and evaporation (Dominguez et al., 2006, 2008; Gimeno et al., 2012), (ii) increased antecedent precipitation (Koster et al., 2004), and (iii) increased water on the land due to agriculture activity (Kustu et al., 2011). In the full NAM region (southwest United States and Mexico), Mahalov et al. (2016) found irrigation to have a positive impact on the rainfall in eastern Arizona-western

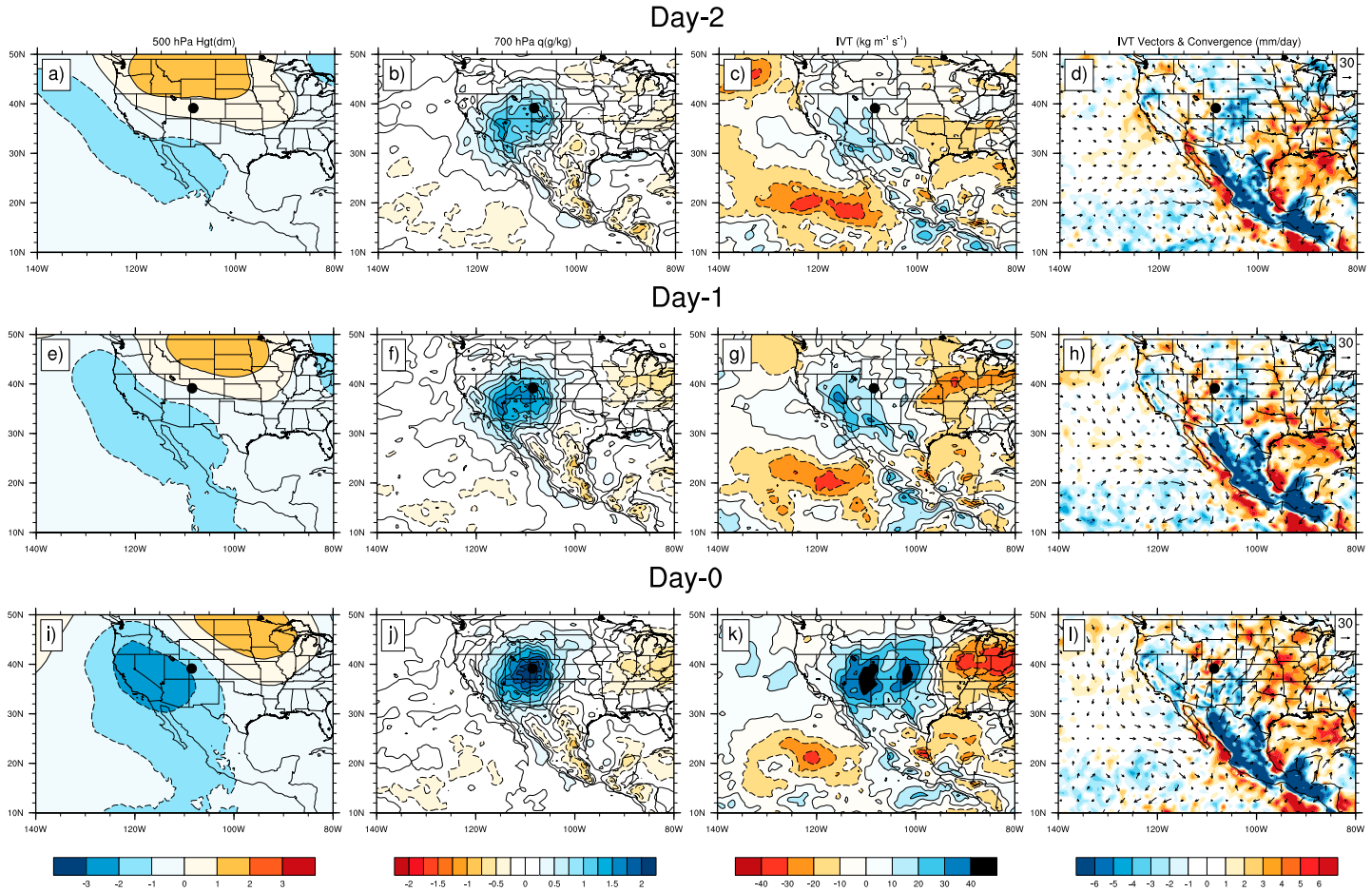

Figure 9. Same as Figure 8 but for Grand Junction, CO trajectories originating from Land.

New Mexico and in northwestern Mexico. An increase in irrigation leads to increases in evapotranspiration, surface mixing ratios, and vertical vapor fluxes, thus causing an increase in precipitation. Bohn and Vivoni (2017), however, argued that the use of an outdated land cover map and misidentification of irrigated pixels in Mahalov et al. (2016) could have resulted in a substantial overestimation of the impact of agricultural irrigation in parts like Chihuahua and regions surrounding the GoC. Agricultural irrigation has also been found to impact monsoons in other parts of the world such as the Asian Monsoon (E. M. Douglas et al., 2006; Saeed et al., 2009) and the African Monsoon (Alter et al., 2015; Im et al., 2014; Im & Eltahir, 2014).

To investigate the differences in the trajectory characteristics associated with rain events from these sources, we calculated the overall speed of each trajectory using the sum of distances traveled at hourly time steps over the 72-hr period. Figure 7 shows the overall speeds of trajectories from the four sources arriving at the six stations. Overall, the trajectories traveling from the Pacific Ocean, GoC, and GoM had relatively higher speeds compared to those from land, although the speed can have more complex behavior at the mesoscale level. Trajectories with the highest speeds were found to be extreme events originating from the Pacific and passing over the GoC. The speeds of these trajectories were comparable to the maximum wind speeds near the surface (300–600 m AGL) in the Gulf low-level jet as observed by M. W. Douglas (1995) and the southeasterly winds over the GoC which have an average speed of 36 km/hr (Mejia et al., 2016). We also compared the speeds between trajectories that produced extreme rainfall (i.e., above the 85th percentile) and others and found no discernable differences in trajectories, suggesting that they were modulated by similar large-scale mechanisms.

4.4. Large-Scale Circulation

Large-scale circulation features influence moisture transport and summer rainfall in this domain. To identify this connection, we constructed composite maps of anomalous 500-mb geopotential height, 700-mb specific

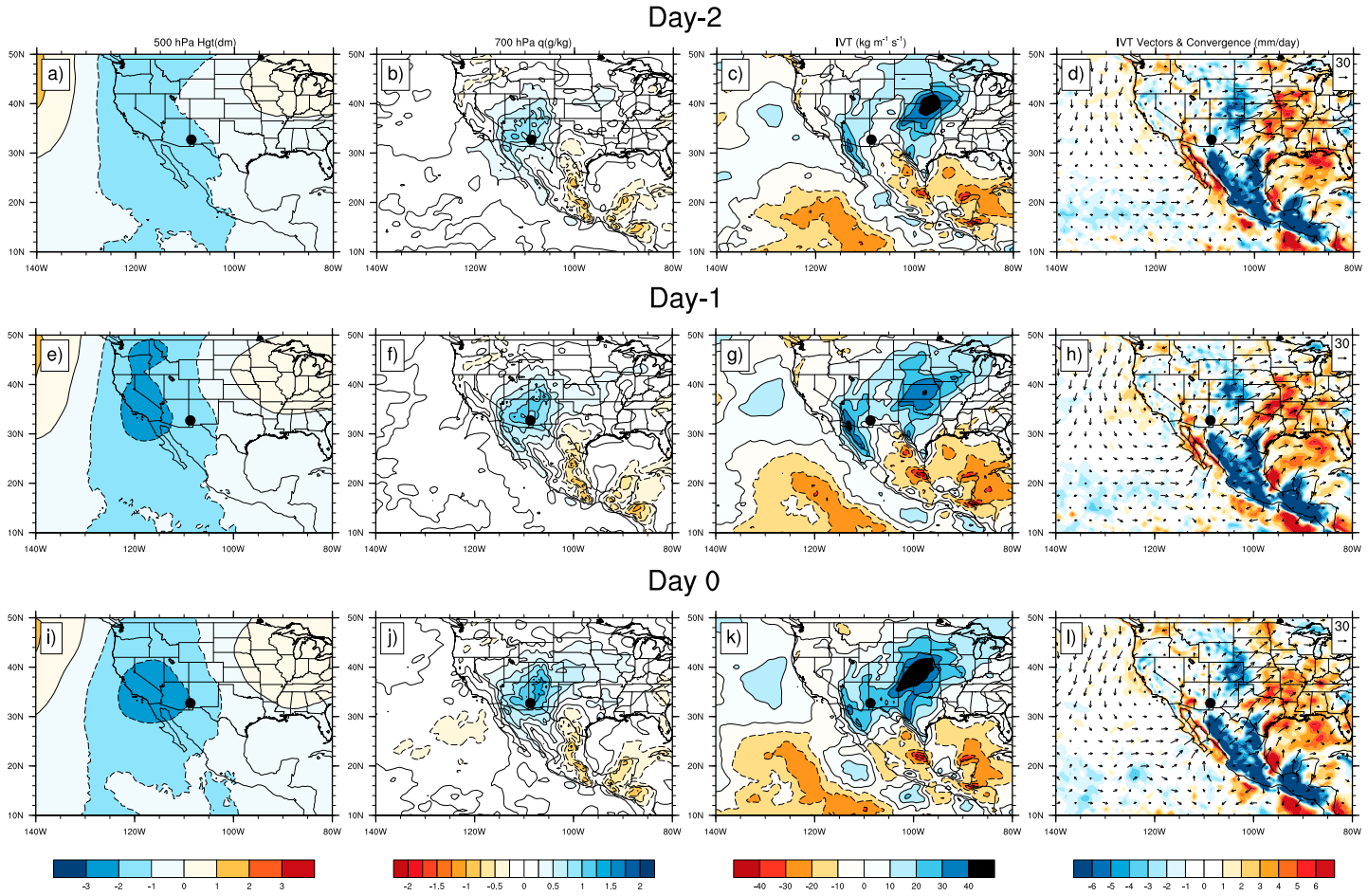

Figure 10. Same as Figure 8 but for Redrock, NM trajectories originating from Gulf of California.

humidity, IVT, and moisture convergence for rainfall events at each of the six locations, originating from the dominant moisture sources. These pressure levels were chosen based on previous studies such as D. K. Adams and Souza (2009). We also investigated other levels, and the results were consistent with those presented here. Furthermore, the composites were plotted for the day of the rainfall event (Day 0) and the preceding 2days—Day-1 and Day-2, respectively, to show the progression of the circulation features. Figure 8 shows the composite maps for rainfall events originating from the GoC at Cedar City. Two days prior to a rainfall event, an anomalous low-pressure pattern begins to develop along the coast of southern California (Figure 8a) with moisture advecting from the GoC (Figures 8c and 8d) which results in higher amounts of moisture over the entire southwest United States (Figure 8b; consistent with the low-pressure pattern). Note that in all the IVT composite maps in this figure and subsequent figures, the moisture convergence is indicated as positive anomalies (red shading) and divergence as negative (blue). Over the next 2 days, this anomalous system intensifies in magnitude and helps transport enhanced moisture from the GoC producing rainfall on day 0 (Figures 8e–8h and 8i–8l).

At Grand Junction, land is the dominant source of moisture; Figure 9 shows the composite maps of the circulation fields for trajectories originating from the land. Here an anomalous low-pressure center extending from northwest Mexico to the Pacific develops 2 days prior to the rainfall event (Figure 9a), with moisture to its east, that is, western Colorado (Figures 9b and 9c) and a consistent moisture transport (Figure 9d) from the NAM region. These patterns intensify in Day-1 and the day of rainfall, Day-0 (Figures 9e–9l). Similarly, for Eastonville, where land is the dominant source, the circulation patterns are consistent with increased vapor transport from northeasterly direction during the day of the rainfall and prior (not shown here). It is worth noting the similarity in the composite maps for Cedar City and Grand Junction; this could be due to the misidentification of GoC trajectories as land trajectories. Since we are only looking at 72 hr before an event, it is

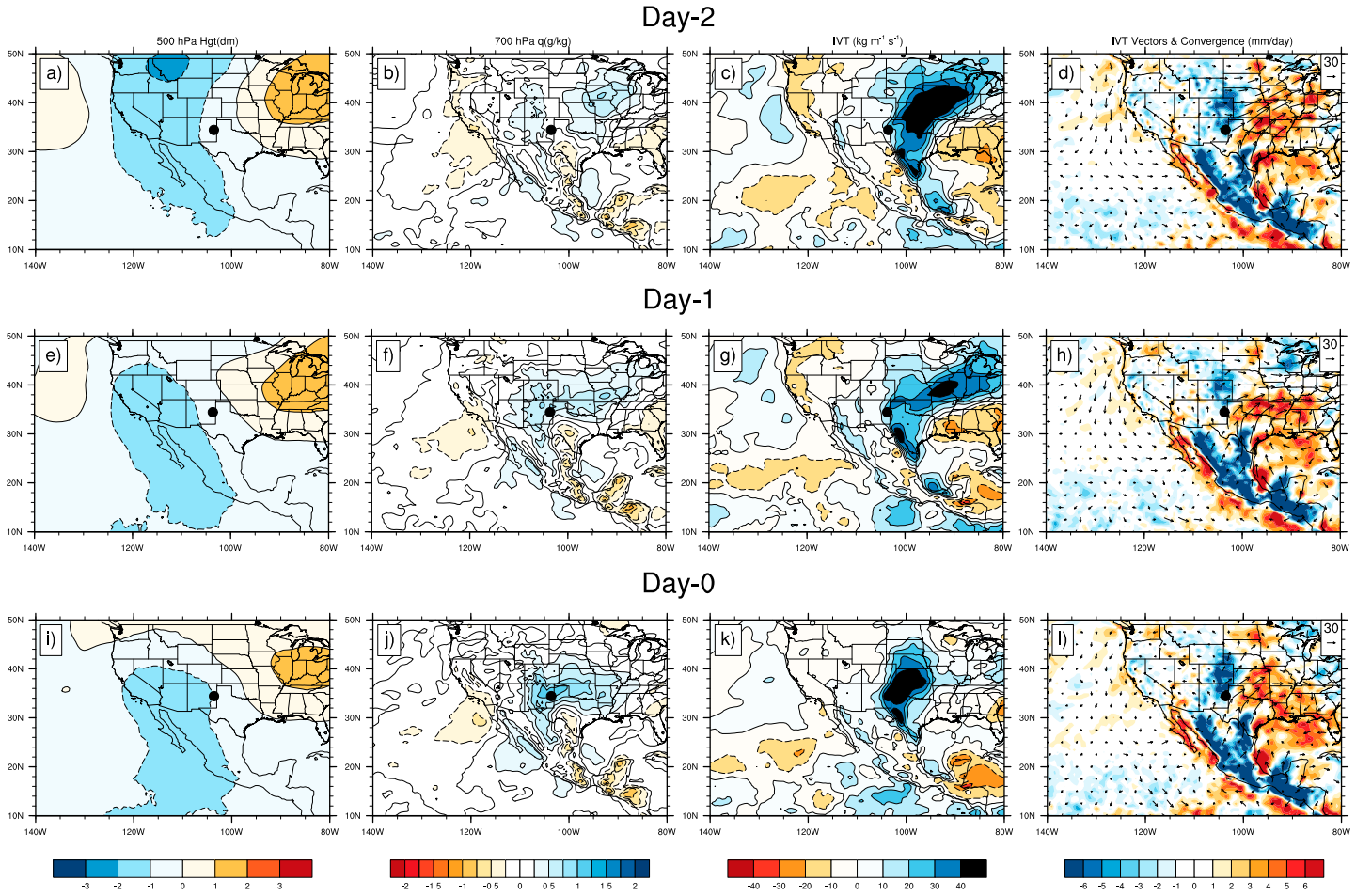

Figure 11. Same as Figure 8 but for Melrose, NM trajectories originating from of Mexico.

possible that some of the land trajectories were, in fact, starting out as oceanic trajectories say 96 or 120 hr before an event.

Figure 10 shows the composite maps for Redrock rainfall trajectories originating from the GoC. These events are marked by anomalous low pressure over southern California and Nevada (Figure 10a) and vapor transport through the GoC (Figures 10b and 10c). Two days prior to rainfall events, the GoC coast experiences an increase in moisture convergence (Figure 10d), which then intensifies through the day of the rainfall (Figures 10e–10l).

For Melrose, the dominant source of precipitation is from the GoM and the composite maps for these trajectories are shown in Figure 11. Two days prior, low-pressure anomalies are seen over the western United States with higher pressures in the eastern United States (Figure 11a). This enables a strong flow of moisture in between these pressure regions which includes Melrose (Figures 11b–11d). The anomalous low pressure in the west reduces to southwest United States, thereby focusing the moisture transport on the day of the rainfall (Figures 11i–11l). Overall in Figures 8–11, the circulation patterns are quite stationary during the 3 days of rainfall and 2 days prior, with progressive intensification toward the day of rainfall. Total convergence maps are provided in the supporting information (Figures S14–S19); however, convergence patterns are very localized and thus conclusions.

5. Conclusions

In this study, we examined the origins and transport of moisture into the southwestern United States to produce summer season rainfall (June–September). We used the Lagrangian particle tracking model,

HYSPLIT, to generate moisture trajectories 3 days backward in time for every rainfall event that occurred during the period 1979 to 2013. The HYSPLIT model was run for six representative stations in the Southwest United States covering the monsoon regions—Cedar City (Great Basin), Grand Junction (Rocky Mountains), Laveen (arid Arizona), Redrock (Core Monsoon), Eastonville, and Melrose (Plains). The dominant source regions for the trajectories were defined to be the GoC, GoM, land, and the Pacific Ocean. The dominant sources and trajectories, however, vary widely over southwestern United States. We can broadly infer the following conclusions. In western Arizona and Utah, GoC and Pacific are the main sources of moisture and the trajectories to this region travel along the GoC. Moving eastward toward eastern Utah and western Colorado, GoC delivers most of the moisture with the core NAM land sources providing the rest. Over eastern Colorado, land evaporation contributes majority of the moisture with GoC making a small contribution. During the monsoon season, there is an abrupt increase in vegetation levels followed by an increase in the rate of evaporation (Vivoni et al., 2008). This results in an increase in precipitation, thus creating a positive feedback. This helps corroborate the recent findings by Bracken et al. (2015)—antecedent (preceding winter and spring) precipitation and land irrigation are the main sources of moisture from land during summer. Eastern New Mexico gets its moisture almost entirely from GoM, while western New Mexico and eastern Arizona get moisture from GoM and GoC. These continental regions with a single moisture source or two dominant sources maybe exposed to sharp changes in the water cycle and extreme droughts due to changing climate and natural variability than those that receive moisture from multiple sources (Gimeno et al., 2012). Our findings are consistent with those from earlier studies, in that the GoC and Eastern Pacific are the key moisture sources for this region. Although the HYSPLIT model provides us a quantitative representation of the moisture sources, it is unable to model mixing due to deep convection, and this can be a major drawback for regions like the SMO. More refined analyses can be performed as reanalyses continue to improve.

Overall, we found that almost all the moisture was carried in the lower altitudes above local topography of the trajectories. Close to 50% of the trajectories of extreme rainfall events (defined as above the 85th percentile) originated from the leading source of moisture for the respective stations. The trajectories traveling from the GoC and Pacific were found to be fastest, while those from land were the slowest. While land evaporation was the dominant source for eastern Colorado, it played a modest role at other locations, especially in Arizona, Utah, and western New Mexico—furthermore, there was an increasing trend in rainfall from land source at all these locations, in particular eastern Colorado. This increasing rainfall trend, perhaps, could be assisted by the general land warming trend. Despite its small size, the GoC plays an important role in providing moisture for good part of the region (Arizona, Utah, western Colorado, and New Mexico).

Summer rainfall over southwestern United States is an important source of moisture for water supply and socioeconomic activity in this semiarid region. While winter precipitation provides bulk of the water for the region, summer contribution is not insignificant as it can help replenish streams after a dry winter. However, unlike winter precipitation, it is highly variable and less predictable, thus frustrating efforts to incorporate it in water resources and agricultural planning. To help in this effort, this study makes an important contribution by systematically investigating the moisture sources and trajectories of summer rainfall over southwestern United States. The mosaic of moisture sources and trajectories control the variability and potentially the predictability of summer rainfall. The trajectories generated can be sampled along with climatological and synoptic predictors to identify changes in the intensity of extreme rainfall events, tropical cyclones (DeMaria & Kaplan, 1994), cyclone landfall rates (Yonekura & Hall, 2011), and to evaluate existing hurricane intensity prediction schemes (DeMaria et al., 2005). Also, these trajectories can be coupled with spatial extremes model (Cooley et al., 2007; Cooley & Sain, 2010; Davison et al., 2012) to generate return level maps for extreme precipitation. The findings from this study offer several useful insights that can be explored further to develop skillful summer rainfall forecasting systems to help with efficient water resources management.

Acknowledgments
We wish to gratefully acknowledge support from the National Science Foundation grant 1243270 and in-kind funding for Andrea J. Ray from the NOAA/ESRL Physical Sciences Division. We thank David K. Adams and an anonymous reviewer for their extensive and insightful comments which helped improve the manuscript significantly. Our reviewers suggested using high-resolution reanalysis instead of NCEP-NCAR Reanalysis 1 for running the HYSPLIT model. We also thank Jon Eischeid and James Scott of NOAA/ESRL/PSD and Cameron Bracken, formerly of University of Colorado at Boulder, for help with acquiring data and scripts for plotting. We also thank Joseph Barsugli, Martin Hoerling, Prashant Sardeshmukh, and Richard Seager, and the Attribution and Predictability Assessments team at NOAA/ESRL/PSD for their inputs on earlier drafts. The NARR data set used for generating the trajectories is available from the NOAA ARL ftp server (ftp://arlftp.arlhq.noaa.gov/narr). The trajectories generated using HYSPLIT and NARR can be accessed at http://civil.colorado.edu/~balajir/sjana/.

References

Adams, D. K., & Comrie, A. C. (1997). The North American Monsoon. *Bulletin of the American Meteorological Society*, *78*(10), 2197–2213. https://doi.org/10.1175/1520-0477(1997)078%3C2197:TNAM%3E2.0.CO;2

Adams, D. K., & Souza, E. P. (2009). CAPE and convective events in the southwest during the North American monsoon. *Monthly Weather Review*, *137*(1), 83–98. https://doi.org/10.1175/2008MWR2502.1

Adams, D. K., Vivoni, E. R., Lintner, B. R., Minjarez Sosa, C., Serra, Y. L., Granados, A., et al. (2018). The North American Monsoon GPS Hydrometeorological Network 2017, in AMS 98th Annual Meeting Conference Abstracts.

Adams, J. L., & Stensrud, D. J. (2007). Impact of tropical easterly waves on the North American monsoon. *Journal of Climate*, *20*(7), 1219–1238. https://doi.org/10.1175/JCLI4071.1

Adang, T. C., & Gall, R. L. (1989). Structure and dynamics of the Arizona monsoon boundary. *Monthly Weather Review*, *117*(7), 1423–1438. https://doi.org/10.1175/1520-0493(1989)117%3C1423:SADOTA%3E2.0.CO;2

Alessandri, A., & Navarra, A. (2008). On the coupling between vegetation and rainfall inter-annual anomalies: Possible contributions to seasonal rainfall predictability over land areas. *Geophysical Research Letters*, *35*, L02718. https://doi.org/10.1029/2007GL032415

Alter, R. E., Im, E. S., & Eltahir, E. A. (2015). Rainfall consistently enhanced around the Gezira Scheme in East Africa due to irrigation. *Nature Geoscience*, *8*(10), 763–767. https://doi.org/10.1038/ngeo2514

Anderson, B. T., Roads, J. O., Chen, S. C., & Juang, H. M. H. (2001). Model dynamics of summertime low-level jets over northwestern Mexico. *Journal of Geophysical Research*, *106*(D4), 3401–3413. https://doi.org/10.1029/2000JD900491

Araguás-Araguás, L., Froehlich, K., & Rozanski, K. (1998). Stable isotope composition of precipitation over southeast Asia. *Journal of Geophysical Research*, *103*(D22), 28,721–28,742. https://doi.org/10.1029/98JD02582

Badan-Dangon, A., Dorman, C. E., Merrifield, M. A., & Winant, C. D. (1991). The lower atmosphere over the Gulf of California. *Journal of Geophysical Research*, *96*(C9), 16,877–16,896. https://doi.org/10.1029/91JC01433

Barlow, M., Nigam, S., & Berbery, E. H. (1998). Evolution of the North American monsoon system. *Journal of Climate*, *11*(9), 2238–2257. https://doi.org/10.1175/1520-0442(1998)011%3C2238:EOTNAM%3E2.0.CO;2

Becker, E. J., Berbery, E. H., & Higgins, R. W. (2009). Understanding the characteristics of daily precipitation over the United States using the North American Regional Reanalysis. *Journal of Climate*, *22*(23), 6268–6286. https://doi.org/10.1175/2009JCLI2838.1

Benton, G. S., & Estoque, M. A. (1954). Water-vapor transfer over the North American continent. *Journal of Meteorology*, *11*(6), 462–477. https://doi.org/10.1175/1520-0469(1954)011%3C0462:WVTOTN%3E2.0.CO;2

Bieda, S. W., Castro, C. L., Mullen, S. L., Comrie, A. C., & Pytlak, E. (2009). The relationship of transient upper-level troughs to variability of the North American monsoon system. *Journal of Climate*, *22*(15), 4213–4227. https://doi.org/10.1175/2009JCLI2487.1

Bohn, T. J., & Vivoni, E. R. (2017). Comment on "Regional impacts of irrigation in Mexico and southwestern US on hydrometeorological fields in the North American Monsoon region," by Mahalov et al. (2016). *Journal of Hydrometeorology*, *19*, 477–481. https://doi.org/10.1175/JHM-D-16-0297.1

Bosilovich, M. G., Sud, Y. C., Schubert, S. D., & Walker, G. K. (2003). Numerical simulation of the large-scale North American monsoon water sources. *Journal of Geophysical Research*, *108*(D16), 8614. https://doi.org/10.1029/2002JD003095

Bottyán, E., Czuppon, G., Kármán, K., Weidinger, T., & Haszpra, L. (2014). Moisture source diagnostic for Hungary based on trajectory analysis and stable isotopic composition of precipitation, in EGU General Assembly Conference Abstracts, vol. 16, p. 2014.

Bracken, C., Rajagopalan, B., Alexander, M., & Gangopadhyay, S. (2015). Spatial variability of seasonal extreme precipitation in the western United States. *Journal of Geophysical Research: Atmospheres*, *120*, 4522–4533. https://doi.org/10.1002/2015JD023205

Brenner, I. S. (1974). A surge of maritime tropical air—Gulf of California to the southwestern United States. *Monthly Weather Review*, *102*(5), 375–389. https://doi.org/10.1175/1520-0493(1974)102%3C0375:ASOMTA%3E2.0.CO;2

Brubaker, K. L., Dirmeyer, P. A., Sudradjat, A., Levy, B. S., & Bernal, F. (2001). A 36-yr climatological description of the evaporative sources of warm-season precipitation in the Mississippi River basin. *Journal of Hydrometeorology*, *2*(6), 537–557. https://doi.org/10.1175/1525-7541(2001)002%3C0537:AYCDOT%3E2.0.CO;2

Bryson, R. A. (1955). *The synoptic climatology of the Arizona Summer Monsoon*. Madison: University of Wisconsin.

Bukovsky, M. S., & Karoly, D. J. (2007). A brief evaluation of precipitation from the North American Regional Reanalysis. *Journal of Hydrometeorology*, *8*(4), 837–846. https://doi.org/10.1175/JHM595.1

Carleton, A. M. (1986). Synoptic-dynamic character of 'bursts' and 'breaks' in the South-West US summer precipitation singularity. *International Journal of Climatology*, *6*(6), 605–623. https://doi.org/10.1002/joc.3370060604

Carleton, A. M., Carpenter, D. A., & Weser, P. J. (1990). Mechanisms of interannual variability of the southwest United States summer rainfall maximum. *Journal of Climate*, *3*(9), 999–1015. https://doi.org/10.1175/1520-0442(1990)003%3C0999:MOIVOT%3E2.0.CO;2

Cavazos, T., Comrie, A. C., & Liverman, D. M. (2002). Intraseasonal variability associated with wet monsoons in southeast Arizona. *Journal of Climate*, *15*(17), 2477–2490. https://doi.org/10.1175/1520-0442(2002)015%3C2477:IVAWWM%3E2.0.CO;2

Cooley, D., Nychka, D., & Naveau, P. (2007). Bayesian spatial modeling of extreme precipitation return levels. *Journal of the American Statistical Association*, *102*(479), 824–840. https://doi.org/10.1198/016214506000000780

Cooley, D., & Sain, S. R. (2010). Spatial hierarchical modeling of precipitation extremes from a regional climate model. *Journal of Agricultural, Biological, and Environmental Statistics*, *15*(3), 381–402. https://doi.org/10.1007/s13253-010-0023-9

Corbosiero, K. L., Dickinson, M. J., & Bosart, L. F. (2009). The contribution of eastern North Pacific tropical cyclones to the rainfall climatology of the southwest United States. *Monthly Weather Review*, *137*(8), 2415–2435. https://doi.org/10.1175/2009MWR2768.1

Davison, A. C., Padoan, S. A., & Ribatet, M. (2012). Statistical modeling of spatial extremes. *Statistical Science*, *27*(2), 161–186. https://doi.org/10.1214/11-STS376

DeMaria, M., & Kaplan, J. (1994). A statistical hurricane intensity prediction scheme (SHIPS) for the Atlantic basin. *Weather and Forecasting*, *9*(2), 209–220. https://doi.org/10.1175/1520-0434(1994)009%3C0209:ASHIPS%3E2.0.CO;2

DeMaria, M., Mainelli, M., Shay, L. K., Knaff, J. A., & Kaplan, J. (2005). Further improvements to the statistical hurricane intensity prediction scheme (SHIPS). *Weather and Forecasting*, *20*(4), 531–543. https://doi.org/10.1175/WAF862.1

Dirmeyer, P. A., & Brubaker, K. L. (1999). Contrasting evaporative moisture sources during the drought of 1988 and the flood of 1993. *Journal of Geophysical Research*, *104*(D16), 19,383–19,397. https://doi.org/10.1029/1999JD900222

Dirmeyer, P. A., & Brubaker, K. L. (2007). Characterization of the global hydrologic cycle from a back-trajectory analysis of atmospheric water vapor. *Journal of Hydrometeorology*, *8*(1), 20–37. https://doi.org/10.1175/JHM557.1

Dominguez, F., & Kumar, P. (2008). Precipitation recycling variability and ecoclimatological stability—A study using NARR data. Part I: Central US plains ecoregion. *Journal of Climate*, *21*(20), 5165–5186. https://doi.org/10.1175/2008JCLI1756.1

Dominguez, F., Kumar, P., Liang, X.-Z., & Ting, M. (2006). Impact of atmospheric moisture storage on precipitation recycling. *Journal of Climate*, *19*(8), 1513–1530. https://doi.org/10.1175/JCLI3691.1

Dominguez, F., Kumar, P., & Vivoni, E. R. (2008). Precipitation recycling variability and ecoclimatological stability—A study using NARR data. Part II: North American Monsoon region. *Journal of Climate*, *21*(20), 5187–5203. https://doi.org/10.1175/2008JCLI1760.1

Dominguez, F., Miguez-Macho, G., & Hu, H. (2016). WRF with water vapor tracers: A study of moisture sources for the North American Monsoon. *Journal of Hydrometeorology*, *17*(7), 1915–1927. https://doi.org/10.1175/JHM-D-15-0221.1

Dominguez, F., Villegas, J. C., & Breshears, D. D. (2009). Spatial extent of the North American Monsoon: Increased cross-regional linkages via atmospheric pathways. *Geophysical Research Letters*, *36*, L07401. https://doi.org/10.1029/2008GL037012

Douglas, E. M., Niyogi, D., Frolking, S., Yeluripati, J. B., Pielke, R. A., Niyogi, N., et al. (2006). Changes in moisture and energy fluxes due to agricultural land use and irrigation in the Indian Monsoon Belt. *Geophysical Research Letters*, *33*, L14403. https://doi.org/10.1029/2006GL026550

Douglas, M. W. (1995). The summertime low-level jet over the Gulf of California. *Monthly Weather Review*, *123*(8), 2334–2347. https://doi.org/10.1175/1520-0493(1995)123%3C2334:TSLLJO%3E2.0.CO;2

Douglas, M. W., & Leal, J. C. (2003). Summertime surges over the Gulf of California: Aspects of their climatology, mean structure, and evolution from radiosonde, NCEP reanalysis, and rainfall data. *Weather and Forecasting*, *18*(1), 55–74. https://doi.org/10.1175/1520-0434(2003)018%3C0055:SSOTGO%3E2.0.CO;2

Douglas, M. W., Maddox, R. a., Howard, K., & Reyes, S. (1993). The Mexican monsoon. *Journal of Climate*, *6*(8), 1665–1677. https://doi.org/10.1175/1520-0442(1993)006%3C1665:TMM%3E2.0.CO;2

Douglas, M. W., Valdez-Manzanilla, A., & Garcia Cueto, R. (1998). Diurnal variation and horizontal extent of the low-level jet over the northern Gulf of California. *Monthly Weather Review*, *126*(7), 2017–2025. https://doi.org/10.1175/1520-0493(1998)126%3C2017:DVAHEO%3E2.0.CO;2

Draxler, R. R. (1996). Trajectory optimization for balloon flight planning. *Weather and Forecasting*, *11*(1), 111–114. https://doi.org/10.1175/1520-0434(1996)011%3C0111:TOFBFP%3E2.0.CO;2

Draxler, R. R., & Hess, G. D. (1997). Description of the HYSPLIT4 modeling system.

Draxler, R. R., & Hess, G. D. (1998). An overview of the HYSPLIT_4 modelling system for trajectories, dispersion, and deposition. *Australian Meteorological Magazine*, *47*(June 1997), 295–308.

Draxler, R. R., Stunder, B., Rolph, G., Stein, A., & Taylor, A. (2014). HYSPLIT4 user's guide version 4.9, 2009, (September).

Easterling, D. R. (2002). United States historical climatology network daily temperature and precipitation data (1871–1997) (No. ORNL/CDIAC-118). ORNL Oak Ridge National Laboratory (US).

Ek, M. B., Mitchell, K. E., Lin, Y., Rogers, E., Grunmann, P., Koren, V., et al. (2003). Implementation of Noah land surface model advances in the National Centers for Environmental Prediction operational mesoscale Eta model. *Journal of Geophysical Research*, *108*(D22), 8851. https://doi.org/10.1029/2002JD003296

Erfani, E., & Mitchell, D. (2014). A partial mechanistic understanding of the North American monsoon. *Journal of Geophysical Research: Atmospheres*, *119*, 13,096–13,115. https://doi.org/10.1002/2014JD022038

Findell, K. L., Gentine, P., Lintner, B. R., & Kerr, C. (2011). Probability of afternoon precipitation in eastern United States and Mexico enhanced by high evaporation. *Nature Geoscience*, *4*(7), 434–439. https://doi.org/10.1038/ngeo1174

Fuller, R. D., & Stensrud, D. J. (2000). The relationship between tropical easterly waves and surges over the Gulf of California during the North American Monsoon. *Monthly Weather Review*, *128*(8), 2983–2989. https://doi.org/10.1175/1520-0493(2000)128%3C2983:TRBTEW%3E2.0.CO;2

Gimeno, L., Stohl, A., Trigo, R. M., Dominguez, F., Yoshimura, K., Yu, L., et al. (2012). Oceanic and terrestrial sources of continental precipitation. *Reviews of Geophysics*, *50*, RG4003. https://doi.org/10.1029/2012RG000389

Griffiths, P. G., Magirl, C. S., Webb, R. H., Pytlak, E., Troch, P. A., & Lyon, S. W. (2009). Spatial distribution and frequency of precipitation during an extreme event: July 2006 mesoscale convective complexes and floods in southeastern Arizona. *Water Resources Research*, *45*, W07419. https://doi.org/10.1029/2008WR007380

Gustafsson, M., Rayner, D., & Chen, D. (2010). Extreme rainfall events in southern Sweden: Where does the moisture come from? *Tellus A*, *62*(5), 605–616. https://doi.org/10.1111/j.1600-0870.2010.00456.x

Gutzler, D. S. (2004). An index of interannual precipitation variability in the core of the North American monsoon region. *Journal of Climate*, *17*(22), 4473–4480.

Hales, J. E. (1972). Surges of maritime tropical air northward over the Gulf of California. *Monthly Weather Review*, *100*(4), 298–306.

Hales, J. E. (1974). Southwestern United States summer monsoon source—Gulf of Mexico or Pacific Ocean. *Journal of Applied Meteorology*, *13*(3), 331–342. https://doi.org/10.1175/1520-0450(1974)013%3C0331:SUSSMS%3E2.0.CO;2

Higgins, R. W., Chen, Y., & Douglas, a. V. (1999). Interannual variability of the North American warm season precipitation regime. *Journal of Climate*, *12*(3), 653–680. https://doi.org/10.1175/1520-0442(1999)012%3C0653:IVOTNA%3E2.0.CO;2

Higgins, R. W., Mo, K. C., & Yao, Y. (1998). Interannual variability of the US summer precipitation regime with emphasis on the southwestern monsoon. *Journal of Climate*, *11*(10), 2582–2606. https://doi.org/10.1175/1520-0442(1998)011%3C2582:IVOTUS%3E2.0.CO;2

Higgins, R. W., Yao, Y., & Wang, X. L. (1997). Influence of the North American monsoon system on the US summer precipitation regime. *Journal of Climate*, *10*(10), 2600–2622. https://doi.org/10.1175/1520-0442(1997)010%3C2600:IOTNAM%3E2.0.CO;2

Higgins, W., Ahijevych, D., Amador, J., Barros, A., Berbery, E. H., Caetano, E., et al. (2006). The NAME 2004 field campaign and modeling strategy. *Bulletin of the American Meteorological Society*, *87*(1), 79–94. https://doi.org/10.1175/BAMS-87-1-79

Hu, H., & Dominguez, F. (2015). Evaluation of oceanic and terrestrial sources of moisture for the North American monsoon using numerical models and precipitation stable isotopes. *Journal of Hydrometeorology*, *16*(1), 19–35. https://doi.org/10.1175/JHM-D-14-0073.1

Im, E. S., & Eltahir, E. A. (2014). Enhancement of rainfall and runoff upstream from irrigation location in a climate model of West Africa. *Water Resources Research*, *50*, 8651–8674. https://doi.org/10.1002/2014WR015592

Im, E. S., Marcella, M. P., & Eltahir, E. A. (2014). Impact of potential large-scale irrigation on the West African monsoon and its dependence on location of irrigated area. *Journal of Climate*, *27*(3), 994–1009. https://doi.org/10.1175/JCLI-D-13-00290.1

James, P., Stohl, A., Spichtinger, N., Eckhardt, S., & Forster, C. (2004). Climatological aspects of the extreme European rainfall of August 2002 and a trajectory method for estimating the associated evaporative source regions. *Natural Hazards and Earth System Sciences*, *4*(5/6), 733–746. https://doi.org/10.5194/nhess-4-733-2004

Jurwitz, L. R. (1953). Arizona's two-season rainfall pattern. *Weatherwise*, *6*(4), 96–99. https://doi.org/10.1080/00431672.1953.9932951

Kennedy, A. D., Dong, X., Xi, B., Xie, S., Zhang, Y., & Chen, J. (2011). A comparison of MERRA and NARR reanalyses with the DOE ARM SGP data. *Journal of Climate*, *24*(17), 4541–4557. https://doi.org/10.1175/2011JCLI3978.1

Koster, R. D., Dirmeyer, P. A., Guo, Z., Bonan, G., Chan, E., Cox, P., et al. (2004). Regions of strong coupling between soil moisture and precipitation. *Science*, *305*(5687), 1138–1140. https://doi.org/10.1126/science.1100217

Kursinski, E. R., Bennett, R. A., Gochis, D., Gutman, S. I., Holub, K. L., Mastaler, R., et al. (2008). Water vapor and surface observations in northwestern Mexico during the 2004 NAME Enhanced Observing Period. *Geophysical Research Letters*, *35*, L03815. https://doi.org/10.1029/2007GL031404

Kustu, M. D., Fan, Y., & Rodell, M. (2011). Possible link between irrigation in the U.S. High Plains and increased summer streamflow in the Midwest. *Water Resources Research*, *47*, W03522. https://doi.org/10.1029/2010WR010046. Bull. Am. Meteorol. Soc., 87(3), 343.

Leeper, R. D., Bell, J. E., Vines, C., & Palecki, M. (2017). An evaluation of the North American regional reanalysis simulated soil moisture conditions during the 2011–13 drought period. *Journal of Hydrometeorology*, *18*(2), 515–527. https://doi.org/10.1175/JHM-D-16-0132.1

Leung, L. R., Qian, Y., & Bian, X. (2003). Hydroclimate of the western United States based on observations and regional climate simulation of 1981–2000. Part I: Seasonal statistics. *Journal of Climate*, *16*(12), 1892–1911. https://doi.org/10.1175/1520-0442(2003)016%3C1892:HOTWUS%3E2.0.CO;2

Lin, Y., Mitchell, K. E., Rogers, E., Baldwin, M. E., & DiMego, G. J. (1999). Test assimilations of the real-time, multi-sensor hourly precipitation analysis into the NCEP Eta model. In Preprints, 8th Conf. on Mesoscale Meteorology, Boulder, CO, Amer. Meteor. Soc (pp. 341–344).

Liu, Z., Notaro, M., Kutzbach, J., & Liu, N. (2006). Assessing global vegetation–climate feedbacks from observations. *Journal of Climate*, *19*(5), 787–814. https://doi.org/10.1175/JCLI3658.1

Luong, T. M., Castro, C. L., Chang, H. I., Lahmers, T., Adams, D. K., & Ochoa-Moya, C. A. (2017). The more extreme nature of North American Monsoon precipitation in the southwestern United States as revealed by a historical climatology of simulated severe weather events. *Journal of Applied Meteorology and Climatology*, *56*(9), 2509–2529. https://doi.org/10.1175/JAMC-D-16-0358.1

Maddox, R. A., McCollum, D. M., & Howard, K. W. (1995). Large-scale patterns associated with severe summertime thunderstorms over central Arizona. *Weather and Forecasting*, *10*(4), 763–778. https://doi.org/10.1175/1520-0434(1995)010%3C0763:LSPAWS%3E2.0.CO;2

Mahalov, A., Li, J., & Hyde, P. (2016). Regional impacts of irrigation in Mexico and the southwestern United States on hydrometeorological fields in the North American Monsoon region. *Journal of Hydrometeorology*, *17*(12), 2981–2995. https://doi.org/10.1175/JHM-D-15-0223.1

Mazon, J. J., Castro, C. L., Adams, D. K., Chang, H. I., Carrillo, C. M., & Brost, J. J. (2016). Objective climatological analysis of extreme weather events in Arizona during the North American monsoon. *Journal of Applied Meteorology and Climatology*, *55*(11), 2431–2450. https://doi.org/10.1175/JAMC-D-16-0075.1

Meitin, J. G., Howard, K. W., & Maddox, R. A. (1991). Southwest area monsoon project. Daily operations summary, 14.

Mejia, J. F., Douglas, M. W., & Lamb, P. J. (2010). Aircraft observations of the 12–15 July 2004 moisture surge event during the North American Monsoon Experiment. *Monthly Weather Review*, *138*(9), 3498–3513. https://doi.org/10.1175/2010MWR3228.1

Mejia, J. F., Douglas, M. W., & Lamb, P. J. (2016). Observational investigation of relationships between moisture surges and mesoscale-to large-scale convection during the North American monsoon. *International Journal of Climatology*, *36*(6), 2555–2569.

Méndez-Barroso, L. A., & Vivoni, E. R. (2010). Observed shifts in land surface conditions during the North American Monsoon: Implications for a vegetation–rainfall feedback mechanism. *Journal of Arid Environments*, *74*(5), 549–555. https://doi.org/10.1016/j.jaridenv.2009.09.026

Mesinger, F., DiMego, G., Kalnay, E., Mitchell, K., Shafran, P. C., Ebisuzaki, W., et al. (2006). North American regional reanalysis. *Bulletin of the American Meteorological Society*, *87*(3), 343–360. https://doi.org/10.1175/BAMS-87-3-343

Mitchell, D. L., Ivanova, D., & Severe, N. (2002). Gulf of California sea surface temperatures and the North American Monsoon: Mechanistic implications from observations. *Journal of Climate*, *15*(17), 2261–2281. https://doi.org/10.1175/1520-0442(2002)015%3C2261:GOCSST%3E2.0.CO;2

Mo, K. C., & Juang, H. M. (2003). Influence of sea surface temperature anomalies in the Gulf of California on North American monsoon rainfall. *Journal of Geophysical Research*, *108*(D3), 4112. https://doi.org/10.1029/2002JD002403

Mock, C. J. (1996). Climatic controls and spatial variations of precipitation in the western United States. *Journal of Climate*, *9*(5), 1111–1125. https://doi.org/10.1175/1520-0442(1996)009%3C1111:CCASVO%3E2.0.CO;2

Nieto, R., Gimeno, L., & Trigo, R. M. (2006). A Lagrangian identification of major sources of Sahel moisture. *Geophysical Research Letters*, *33*, L18707. https://doi.org/10.1029/2006GL027232

Nigam, S., & Ruiz-Barradas, A. (2006). Seasonal hydroclimate variability over North America in global and regional reanalyses and AMIP simulations: Varied representation. *Journal of Climate*, *19*(5), 815–837. https://doi.org/10.1175/JCLI3635.1

Notaro, M., Liu, Z., & Williams, J. W. (2006). Observed vegetation–climate feedbacks in the United States. *Journal of Climate*, *19*(5), 763–786. https://doi.org/10.1175/JCLI3657.1

Okabe, I. T. (1995). The North American monsoon (Doctoral dissertation, University of British Columbia).

Petterssen, S. (1940). *Weather analysis and forecasting*. New York: McGraw-Hill.

Radhakrishna, B., Fabry, F., Braun, J. J., & Van Hove, T. (2015). Precipitable water from GPS over the continental United States: Diurnal cycle, intercomparisons with NARR, and link with convective initiation. *Journal of Climate*, *28*(7), 2584–2599. https://doi.org/10.1175/JCLI-D-14-00366.1

Rasmusson, E. M. (1966). Atmospheric water vapor transport and the hydrology of North America, (Doctoral dissertation, Massachusetts Institute of Technology).

Rasmusson, E. M. (1967). Atmospheric water vapor transport and the water balance of North America: Part I. *Monthly Weather Review*, *95*(7), 403–426. https://doi.org/10.1175/1520-0493(1967)095%3C0403:AWVTAT%3E2.3.CO;2

Rasmusson, E. M. (1968). Atmospheric water vapor transport and the water balance of North America. *Monthly Weather Review*, *96*(10), 720–734. https://doi.org/10.1175/1520-0493(1968)096%3C0720:AWVTAT%3E2.0.CO;2

Ray, A. J., Garfin, G. M., Wilder, M., Vásquez-León, M., Lenart, M., & Comrie, A. C. (2007). Applications of monsoon research: Opportunities to inform decision making and reduce regional vulnerability. *Journal of Climate*, *20*(9), 1608–1627. https://doi.org/10.1175/JCLI4098.1

Reitan, C. H. (1957). The role of precipitable water vapor in Arizona's summer rains. Tech. Rep. on the Meteorology and Climatology of Arid Regions 2, The Institute of Atmospheric Physics, The University of Arizona, Tucson (19 pp.). [Available from The Institute of Atmospheric Physics, The University of Arizona, Tucson, AZ 85721.]

Reyes, S., & Cadet, D. L. (1986). Atmospheric water vapor and surface flow patterns over the tropical Americas during May–August 1979. *Monthly Weather Review*, *114*(3), 582–593. https://doi.org/10.1175/1520-0493(1986)114%3C0582:AWVASF%3E2.0.CO;2

Reyes, S., & Cadet, D. L. (1988). The southwest branch of the North American Monsoon during summer 1979. *Monthly Weather Review*, *116*(5), 1175–1187. https://doi.org/10.1175/1520-0493(1988)116%3C1175:TSBOTN%3E2.0.CO;2

Reyes, S., Cadet, L., Douglas, M., & Maddox, R. (1994). El monzón del suroeste de Norteamérica (TRAVASON/SWAMP). *Atmosfera*, *7*, 117–137.

Ropelewski, C. F., Gutzler, D. S., Higgins, R. W., & Mechoso, C. R. (2005). The North American monsoon system. The Global Monsoon System: Research and forecast. *WMO Tech. Doc.*, *1266*, 207–218.

Ruiz-Barradas, A., & Nigam, S. (2006). Great Plains hydroclimate variability: The view from North American regional reanalysis. *Journal of Climate*, *19*(12), 3004–3010. https://doi.org/10.1175/JCLI3768.1

Ruiz-Barradas, A., & Nigam, S. (2013). Atmosphere–land surface interactions over the Southern Great Plains: Characterization from pentad analysis of DOE ARM field observations and NARR. *Journal of Climate*, *26*(3), 875–886. https://doi.org/10.1175/JCLI-D-11-00380.1

Saeed, F., Hagemann, S., & Jacob, D. (2009). Impact of irrigation on the South Asian summer monsoon. *Geophysical Research Letters*, *36*, L20711. https://doi.org/10.1029/2009GL040625

Saha, S., Moorthi, S., Pan, H. L., Wu, X., Wang, J., Nadiga, S., et al. (2010). The NCEP climate forecast system reanalysis. *Bulletin of the American Meteorological Society*, *91*(8), 1015–1058. https://doi.org/10.1175/2010BAMS3001.1

Salati, E., Dall'Olio, A., Matsui, E., & Gat, J. R. (1979). Recycling of water in the Amazon basin: An isotopic study. *Water Resources Research*, *15*(5), 1250–1258. https://doi.org/10.1029/WR015i005p01250

Serra, Y. L., Adams, D. K., Minjarez-Sosa, C., Moker Jr, J. M., Arellano, A. F., Castro, C. L., et al. (2016). The North American monsoon GPS transect experiment 2013. *Bulletin of the American Meteorological Society*, *97*(11), 2103–2115. https://doi.org/10.1175/BAMS-D-14-00250.1

Sheppard, P. R., Comrie, A. C., Packin, G. D., Angersbach, K., & Hughes, M. K. (1999). The climate of the Southwest. CLIMAS Report Series CL1-99. Institute for the Study of Planet Earth, University of Arizona, Tucson, Arizona.

Sheppard, P. R., Comrie, A. C., Packin, G. D., Angersbach, K., & Hughes, M. K. (2002). The climate of the US Southwest. *Climate Research*, *21*(3), 219–238. https://doi.org/10.3354/cr021219

Sodemann, H., & Stohl, A. (2009). Asymmetries in the moisture origin of Antarctic precipitation. *Geophysical Research Letters*, *36*, L22803. https://doi.org/10.1029/2009GL040242

Stensrud, D. J., Gall, R. L., Mullen, S. L., & Howard, K. W. (1995). Model climatology of the Mexican monsoon. *Journal of Climate*, *8*(7), 1775–1794. https://doi.org/10.1175/1520-0442(1995)008%3C1775:MCOTMM%3E2.0.CO;2

Stensrud, D. J., Gall, R. L., & Nordquist, M. K. (1997). Surges over the Gulf of California during the Mexican monsoon. *Monthly Weather Review*, *125*(4), 417–437. https://doi.org/10.1175/1520-0493(1997)125%3C0417:SOTGOC%3E2.0.CO;2

Stohl, A. (2003). A backward modeling study of intercontinental pollution transport using aircraft measurements. *Journal of Geophysical Research*, *108*(D12), 4370. https://doi.org/10.1029/2002JD002862

Stohl, A., Forster, C., & Sodemann, H. (2008). Remote sources of water vapor forming precipitation on the Norwegian west coast at 60°N—A tale of hurricanes and an atmospheric river. *Journal of Geophysical Research*, *113*, D05102. https://doi.org/10.1029/2007JD009006

Stohl, A., & James, P. (2004). A Lagrangian analysis of the atmospheric branch of the global water cycle. Part I: Method description, validation, and demonstration for the August 2002 flooding in central Europe. *Journal of Hydrometeorology*, *5*(4), 656–678. https://doi.org/10.1175/1525-7541(2004)005%3C0656:ALAOTA%3E2.0.CO;2

Stohl, A., & James, P. (2005). A Lagrangian analysis of the atmospheric branch of the global water cycle. Part II: Moisture transports between Earth's ocean basins and river catchments. *Journal of Hydrometeorology*, *6*(6), 961–984. https://doi.org/10.1175/JHM470.1

Strong, M., Sharp, Z. D., & Gutzler, D. S. (2007). Diagnosing moisture transport using D/H ratios of water vapor. *Geophysical Research Letters*, *34*, L03404. https://doi.org/10.1029/2006GL028307

Tang, M., & Reiter, E. R. (1984). Plateau monsoons of the Northern Hemisphere: A comparison between North America and Tibet. *Monthly Weather Review*, *112*(4), 617–637. https://doi.org/10.1175/1520-0493(1984)112%3C0617:PMOTNH%3E2.0.CO;2

Vera, C., Higgins, W., Amador, J., Ambrizzi, T., Garreaud, R., Gochis, D., et al. (2006). Toward a unified view of the American monsoon systems. *Journal of Climate*, *19*(20), 4977–5000. https://doi.org/10.1175/JCLI3896.1

Vivoni, E. R., Moreno, H. A., Mascaro, G., Rodriguez, J. C., Watts, C. J., Garatuza-Payan, J., & Scott, R. L. (2008). Observed relation between evapotranspiration and soil moisture in the North American monsoon region. *Geophysical Research Letters*, *35*, L22403. https://doi.org/10.1029/2008GL036001

Wernli, B. H., & Davies, H. C. (1997). A Lagrangian-based analysis of extratropical cyclones. I: The method and some applications. *Quarterly Journal of the Royal Meteorological Society*, *123*(538), 467–489. https://doi.org/10.1002/qj.49712353811

Wernli, H. (1997). A Lagrangian-based analysis of extratropical cyclones. II: A detailed case-study. *Quarterly Journal of the Royal Meteorological Society*, *123*(542), 1677–1706. https://doi.org/10.1002/qj.49712354211

Wright, W. E., Long, A., Comrie, A. C., Leavitt, S. W., Cavazos, T., & Eastoe, C. (2001). Monsoonal moisture sources revealed using temperature, precipitation, and precipitation stable isotope timeseries. *Geophysical Research Letters*, *28*(5), 787–790. https://doi.org/10.1029/2000GL012094

Yamanaka, T., Tsujimura, M., Oyunbaatar, D., & Davaa, G. (2007). Isotopic variation of precipitation over eastern Mongolia and its implication for the atmospheric water cycle. *Journal of Hydrology*, *333*(1), 21–34. https://doi.org/10.1016/j.jhydrol.2006.07.022

Yonekura, E., & Hall, T. M. (2011). A statistical model of tropical cyclone tracks in the western North Pacific with ENSO-dependent cyclogenesis. *Journal of Applied Meteorology and Climatology*, *50*(8), 1725–1739. https://doi.org/10.1175/2011JAMC2617.1